Contrib Mineral Petrol (2001) 140: 680–700
DOI 10.1007/s004100000214

A. K. Schmitt · S. L. de Silva · R. B. Trumbull
R. Emmermann

Magma evolution in the Purico ignimbrite complex, northern Chile: evidence for zoning of a dacitic magma by injection of rhyolitic melts following mafic recharge

Received: 4 May 2000 / Accepted: 18 October 2000 / Published online: 16 January 2001

Abstract The 1.3 Ma Purico complex is part of an extensive Neogene–Pleistocene ignimbrite province in the central Andes. Like most other silicic complexes in the province, Purico is dominated by monotonous intermediate ash-flow sheets and has volumetrically minor lava domes. The Purico ignimbrites (total volume 80–100 km^3) are divided into a Lower Purico Ignimbrite (LPI) with two extensive flow units, LPI I and LPI II; and a smaller Upper Purico Ignimbrite (UPI) unit. Crystal-rich dacite is the dominant lithology in all the Purico ignimbrites and in the lava domes. It is essentially the only lithology present in the first LPI flow unit (LPI I) and in the Upper Purico Ignimbrite, but the LPI II flow unit is unusual for its compositional diversity. It constitutes a stratigraphic sequence with a basal fall-out deposit containing rhyolitic pumice (68–74 wt% SiO_2) overlain by ignimbrite with dominant crystal-rich dacitic pumice (64–66 wt% SiO_2). Rare andesitic and banded pumice (60–61 wt% SiO_2) are also present in the uppermost part of the flow unit. The different compositional groups of pumice in LPI II flow unit (rhyolite, andesite, dacite) have initial Nd and Sr isotopic compositions that are indistinguishable from each other and from the dominant dacitic pumice ($\epsilon Nd = -6.7$ to -7.2 and $^{87}Sr/^{86}Sr = 0.7085$–0.7090). However, two lines of evidence show that the andesite, dacite and rhyolite pumices do not represent a simple fractionation series. First, melt inclusions trapped in sequential growth zones of zoned plagioclase grains in the rhyolite record fractionation trends in the melt that diverge from those shown by dacite samples. Second, mineral equilibrium geothermometry reveals that dacites from all ignimbrite flow units and from the domes had relatively uniform and moderate pre-eruptive temperatures (780–800 °C), whereas the rhyolites and andesites yield consistently higher temperatures (850–950 °C). Hornblende geobarometry and pressure constraints from H_2O and CO_2 contents in melt inclusions indicate upper crustal (4–8 km) magma storage conditions. The petrologic evidence from the LPI II system thus indicates an anomalously zoned magma chamber with a rhyolitic cap that was hotter than, and chemically unrelated to, the underlying dacite. We suggest that the hotter rhyolite and andesite magmas are both related to an episode of replenishment in the dacitic Purico magma chamber. Rapid and effective crystal fractionation of the fresh andesite produced a hot rhyolitic melt whose low density and viscosity permitted ascent through the chamber without significant thermal and chemical equilibration with the resident dacite. Isotopic and compositional variations in the Purico system are typical of those seen throughout the Neogene ignimbrite complexes of the Central Andes. These characteristics were generated at moderate crustal depths (< 30 km) by crustal melting, mixing and homogenization involving mantle-derived basalts. For the Purico system, assimilation of at least 30% mantle-derived material is required.

Electronic supplementary material to this paper can be obtained electronically by using the SPRINGER LINK server located at http://dx.doi.org/10.1007/s004100000214.

A. K. Schmitt (✉)
GeoForschungsZentrum Potsdam, Telegrafenberg,
14473 Potsdam, Germany

S. L. de Silva
Dept. of Geography, Geology, and Anthropology,
Indiana State University, Terre Haute, IN 47809, USA

R. B. Trumbull
GeoForschungsZentrum Potsdam, Telegrafenberg,
14473 Potsdam, Germany

R. Emmermann
Institut für Geowissenschaften und Lithosphärenforschung,
Universität Giessen, 35390 Giessen, Germany

A. K. Schmitt
Present address:
Dept. of Earth and Space Sciences,
University of California Los Angeles,
Los Angeles, CA 90095, USA
e-mail: axel@argon.ess.ucla.edu
Tel.: +1-310-7945047; Fax: +1-310-8252770

Editorial responsibility: J. Hoefs

Introduction

Long-lived episodes of large-scale explosive silicic volcanism mark an important evolutionary stage in the development of continental arcs, e.g., western USA (Lipman et al. 1978; Gans et al. 1989; Best et al. 1995), Sierra Madre Occidental in Mexico (McDowell et al. 1979) and Altiplano-Puna Volcanic Complex, central Andes (de Silva 1989a, 1989b). The climactic eruptions that characterize such episodes typically result in the formation of large caldera complexes and deposition of large-volume regionally extensive ignimbrites. Such events are also viewed as the surface manifestation of large-scale plutonic activity at depth. The tectono-magmatic processes that lead to such so-called ignimbrite "flare-ups" (Elston 1984; de Silva 1989a) are not well understood but they are clearly important for heat and mass transfer within the crust, and modification of crustal composition and structure.

Although many ignimbrites show evidence of compositional zonation or variability, the largest volume ignimbrites rarely do. These are the so-called monotonous intermediates (Smith 1979; Hildreth 1981; de Silva 1991). Hildreth (1981) convincingly argued that the lower regions of crustal silicic magma systems are generally basaltic and that the degree of zonation displayed may be a function of eruptive draw-up, i.e., large systems appear homogeneous because the lower, more mafic layers are rarely evacuated during eruption. Basic recharge may therefore be a fundamental process in large silicic magmatic systems even if only a few studies have conclusively demonstrated its role in producing compositional heterogeneity and influencing the evolution of the system.

The late Tertiary Altiplano–Puna Volcanic Complex (APVC) between 21 and 24°S in the central Andes is exceptionally well preserved because of the prevailing arid climate. The volcanic output of the last 10 million years is volumetrically dominated by crystal-rich dacitic ignimbrites and lavas that range in volume from 10s–100s of km^3, to $> 1000\ km^3$ and form regionally extensive sheets (Fig. 1). The largest ignimbrite sheets were erupted from giant resurgent caldera complexes (e.g., Sparks et al. 1985; Gardeweg and Ramirez 1987; de Silva and Francis 1991; Lindsay et al. 2000). Some moderate volume dacitic ignimbrites are not associated with typical caldera morphologies but form ignimbrite "shields" (Francis and Baker 1978; de Silva and Francis 1991), which are poorly understood as a group (e.g., Lipman 1997). Most APVC ignimbrites are homogeneous; only rarely have rhyolitic units been found in the erupted sequences, and andesitic compositions are likewise scarce (de Silva 1991; Lindsay et al. 2000). The Purico complex in Northern Chile (Figs. 1 and 2) is an important exception wherein rhyolitic and andesitic compositions were erupted along with the dominant dacite (Francis et al. 1984). This, coupled with the fact that the ignimbrites are well exposed and the compositional range of the juvenile material spans that of the APVC, has motivated several petrological and geochemical studies of the Purico complex. These have debated the relative roles of crustal anatexis, closed-system and open-system processes in the origin and evolution of the magmas (Hawkesworth et al. 1982; Francis et al. 1984; Davidson et al. 1990). In a reconnaissance study, de Silva (1991) argued that the compositional zonation at Purico was largely the result of closed system fractional crystallization (convective fractionation). This paper presents the results of a geochemical and petrologic re-examination of the Purico complex based on a stratigraphically well-constrained suite of samples for which we provide new whole-rock major and trace element data. Mineral and glass phases (matrix and melt inclusions) were analyzed to determine pre-eruptive temperature, pressure, and volatile contents. The results suggest that mafic magma recharge was instrumental in the development of the compositional heterogeneity and perhaps also in triggering the eruption. Finally, we examine the petrogenesis of the Purico magmatic center in the broader context of large-scale silicic magmatism in the central Andes.

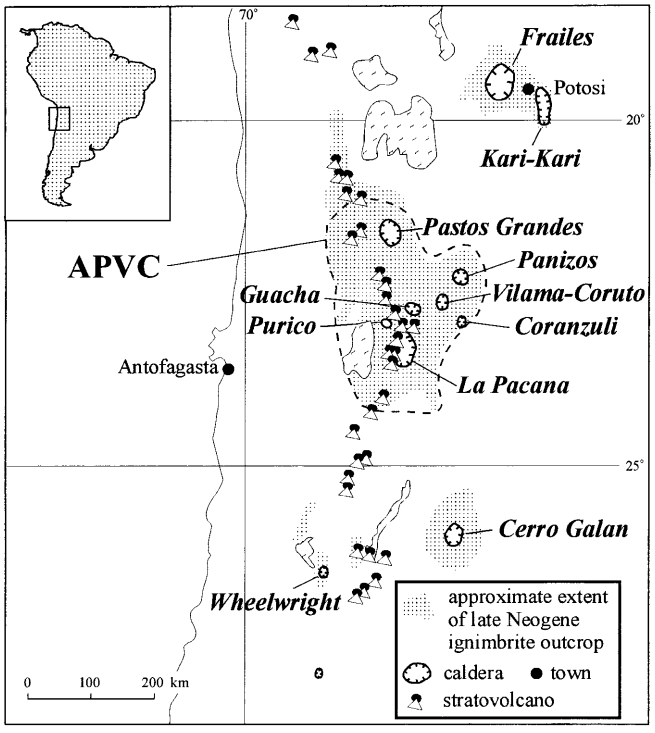

Fig. 1 Map of the distribution of Neogene and Pleistocene ignimbrites in the central Andes. Major calderas and Pleistocene-recent stratovolcanoes of the active arc are also shown (redrawn after de Silva and Francis 1991). The extent of the Altiplano–Puna Volcanic Complex (APVC, de Silva 1991) is outlined

The Purico complex

Geology

The Purico complex (67°45′W and 22°57′S) comprises an approximately circular apron of three ignimbrite flow

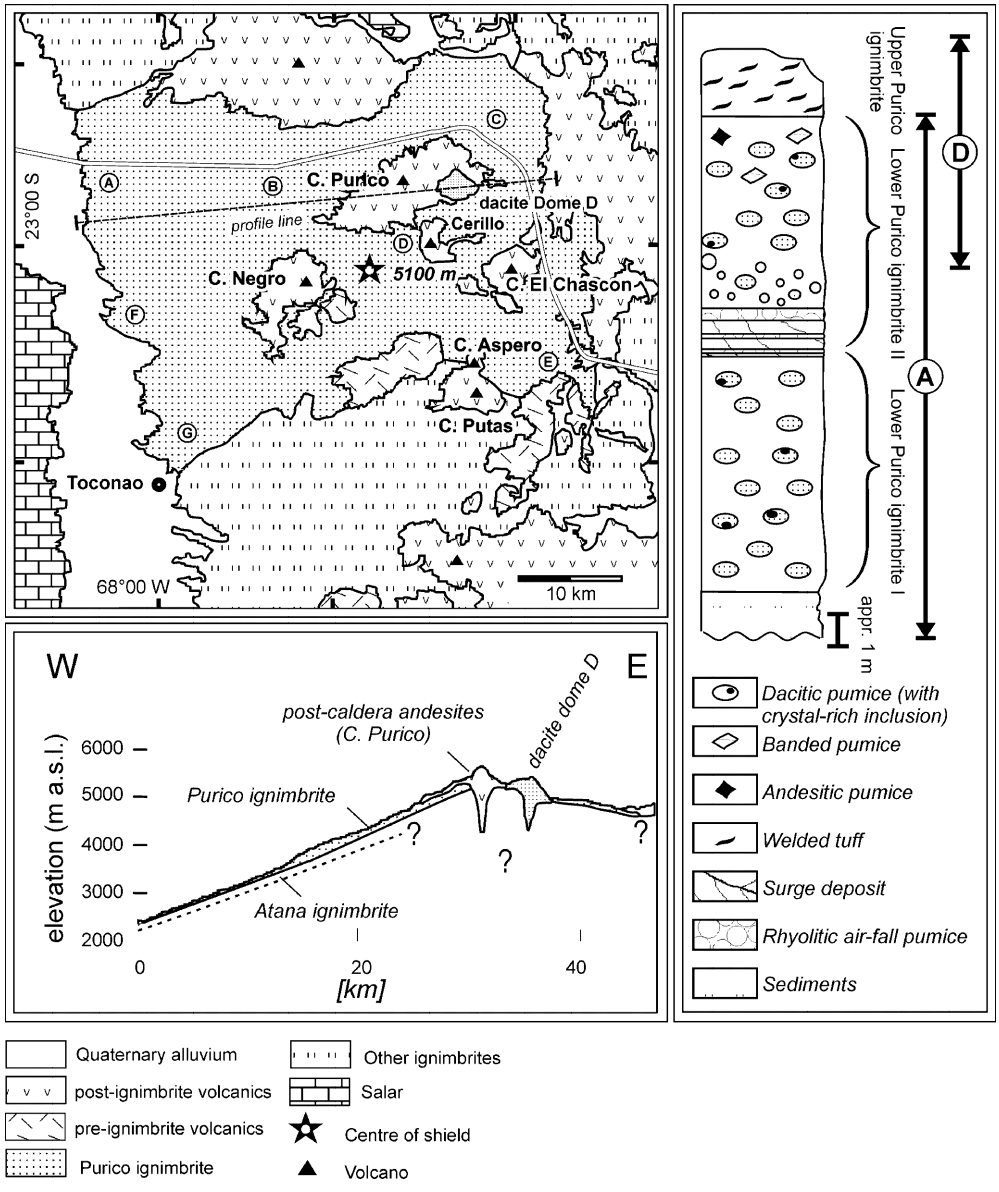

Fig. 2 Geological map, profile and composite stratigraphic column of the Purico Complex. Map and profile made from digital elevation model and Landsat satellite imagery. Inferred vent area is located 2 km SW of Dome D. Sample locations for the Purico ignimbrites and sections in stratigraphic column: *A* Quebrada Corrales Blancos; *B* west of Cerro Purico; *C* Pampa del Vallecito; *D* west of Cerro Chainator; *E* Quebrada Vizcachas; *F* Quebrada Zapar; *G* Quebrada Silapeti

units that are presently exposed over an area of ~15–25 km around the putative vent region. The units dip away from the vent region (5,000 m above sea level) at ~4°, the most prominent dip slope being to the west into the Salar de Atacama basin (Fig. 2). This gives the complex its broad shield-like form. The Purico ignimbrites overlie a major sequence of older ignimbrites that are in part related to the 4.5–4.1 Ma eruptions of the nearby La Pacana caldera (Gardeweg and Ramirez 1987; Lindsay et al. 2000). Published K–Ar ages for the Purico ignimbrite range between 1.38 ± 0.07 and 0.87 ± 0.52 Ma (Francis et al. 1984; de Silva 1989b), the ages overlapping for the different flow-units.

Several dacitic lava domes overly the Purico ignimbrite in the summit region (Dome D, Cerro Purico and El Cerillo), partly surrounding the putative vent for the ignimbrite eruption. On the basis of age and morphology, these domes can be characterized as one of two types. Dome D is a "torta", a flat pancake-shaped flow dome (see Fig. 2) that yielded a biotite K–Ar age within the age range of the ignimbrites (0.98 ± 0.05 Ma; Francis et al. 1984). The Dome D lavas closely resemble the dacite pumice from the ignimbrite in terms of age, mineralogy and chemical composition, suggesting a close genetic relationship for the respective magmas. The other domes (Cerros Purico, Negro, Putas, Chascon, Aspero, and El Cerillo) have conical shapes typical of Peléan domes in the sense of Blake (1990). Radiometric dating of these domes is lacking but the Chascon, Aspero, and El Cerillo domes are clearly post-glacial (Holocene) and their degree of preservation suggests that all are probably < 0.5 Ma old (Francis et al. 1984). Olivine-bearing mafic inclusions are common in the dacite lavas, and they have been interpreted as evidence for magma mingling caused by mafic recharge (Francis et al. 1984; Davidson et al. 1990). Because the young, conical domes

are compositionally distinct from the Purico ignimbrites and the associated Dome D (see Table 1), they are attributed to a separate magmatic event initiated by input of new mafic magma (Hawkesworth et al. 1982; Davidson et al. 1990; Tepley and Davidson 1997).

Stratigraphy of the Purico ignimbrites

We distinguish an Upper (UPI) and Lower Purico Ignimbrite, and further subdivide the Lower Purico Ignimbrite (LPI) into two flow-units designated as LPI I and LPI II for the lower and upper unit, respectively (Fig. 2). The most complete section of the Lower Purico Ignimbrite crops out ~10 km east of the village of San Pedro de Atacama, in quebradas that have unfortunately been mined by the Chilean army, making access to the outcrops interesting.

LPI I is a massive flow unit whereas LPI II comprises a basal surge layer and a normally graded pumice fall deposit, overlain by a pumice-rich flow (Fig. 2). Coarse-grained, dacitic crystal-rich pumice (pl–hbl–bt–qtz ± opx, accessory apa–zrn–sph) is the dominant juvenile component in both LPI flow units. Also present in both flow units are crystal-rich aggregates with a phenocryst assemblage compositionally indistinguishable from the dacite pumice. These aggregates occur as inclusions in dacitic pumice or as individual clasts in the ignimbrite. The LPI II fall deposit is formed by crystal-poor rhyolitic (sensu lato, see below) pumice (pl–bt ± hbl ± opx, accessory apa–zrn), which lacks quartz. The base of the overlying LPI II ash flow also contains clasts of rhyolitic pumice in addition to the dominant dacitic pumice. Dark andesitic and banded dacitic–andesitic pumices (pl–cpx–opx, accessory apa–zrn) appear in the LPI II flow unit and increase in abundance towards the upper part, as does a quartz-poor dacitic variety.

In the Purico summit region close to the putative vent, LPI II is overlain by the matrix-supported Upper Purico ignimbrite (UPI). This moderate to densely welded ignimbrite contains dacitic clasts similar to the LPI II dacitic pumice. Details of the stratigraphic distribution, vesicularity, crystallinity, and modal composition of all pumice types are given in Table 1 and Fig. 2.

The total volume of the Purico ignimbrites has been estimated at ~80–100 km^3 (de Silva 1991). The rhyolitic fall deposit at the base of LPI II was encountered in both of the two accessible localities of the ignimbrite on the western slope of the Purico shield (A and B in Fig. 2) and we assume that it extends throughout this local area. Such fall deposits are commonly associated with a flow unit and the fact that rhyolite pumice is found in the overlying ash flow unit, along with the observation that the fall deposit thickens towards the putative vent, gives us confidence that it is part of the LPI II eruption. If the distribution of the fall deposit coincides with the that of the ignimbrite (1,500 km^2), its total volume is estimated to be 0.4 km^3. The volume of dark pumice is hard to assess given its scarcity in the outcrop, but it is probably $\ll$1% of the total volume of LPI II. The volume of the domes is small compared with the ignimbrite and estimates for individual domes range from 0.36 km^3 for Aspero to ~4 km^3 for Chascon (de Silva and Francis 1991).

Petrology and geochemistry

Whole-rock geochemistry

The emphasis of this study is on the Purico ignimbrites and is based on a total of 36 pumice samples from LPI I, LPI II and UPI (depending on clast size, the samples are single or composite). Sampling covers the vertical and horizontal extent of the deposits (Fig. 2). An additional 13 samples of lava and mafic inclusions from selected domes were included for comparison. We consider the pumice compositions to be representative of magma compositions with the exception of the banded pumices, which resulted from magma mingling, and the crystal-rich inclusions, which are interpreted as cumulates (de Silva 1989c). Bulk matrix samples were excluded because of the likelihood of mechanical fractionation or contamination during eruption and transport. Representative analyses are presented in Table 2 and the full data set is reported in Table 1 of the electronic supplementary material.

The Purico pumices and lavas define a high-K calc-alkaline trend with a total range of SiO_2 from 60 to

Table 1 Vesicularity, phenocryst and glass abundances of Purico–Chascon pumice types and lavas (minimal and maximal values in brackets). Accessory minerals present: zircon, apatite and sphene, the latter only in dacites. See Appendix for analytical methods

Type Unit	Dacitic pumice LPI I and II	Crystal-rich inclusion LPI I and II	Rhyolitic pumice LPI II	Andesitic pumice LPI II	Dacitic lava Dome D	Dacitic lava Chascon-Aspero
Total of samples	8	3	4	6	5	4
Vesicles (vol%)	65	56	72	39	24	–
Glass (wt%)	50 (41,62)	32 (31,33)	80 (78,84)	50 (34,56)	50 (34,58)	30 (23,41)
Pl	70 (66,72)	68 (60,76)	100	56 (49,60)	75 (66,80)	66 (61,71)
Hbl	14 (10,17)	23 (20,28)	< 2	–	14 (10,20)	11 (7,19)
Qtz	11 (7,14)	8 (8,8)	–	–	7 (5,11)	8 (5,10)
Bt	5 (4,9)	6 (4,11)	< 2	–	5 (4,6)	< 2
Opx	< 2	–	< 2	26 (19,30)	< 2	15 (11,22)
Cpx	–	–	–	16 (11,24)	–	–
Others	< 2 Ti-Mag	< 2 Ti-Mag	< 2 Ti-Mag	2 Ti-Mag	< 2 Ti-Mag	< 2 Ti-Mag

Table 2 Major, trace element, Sr and Nd isotopic composition of Purico pumice types (for locations see Fig. 2). Oxides in wt%, traces in ppm. Bulk rock analyses by XRF (Zr, Ba), ICP-MS (Rb, Sr, Y, Nb, Th, U) and ICP-AES (REE). Matrix glass analyses are given for comparison (major elements by EPMA. Water and trace element data on glasses determined by SIMS. –Not analyzed; *dp* dacitic pumice; *dl* dacitic lava; *ci* crystal-rich inclusion; *rp* rhyolitic pumice; *ap* andesitic pumice; *b.d.* below detection)

Sample	PED962H		PED979		PED962D		PED972		PED96H2B	
Unit	LPI II/A		dome D		LPI II/A		LPI II/A		LPI II/B	
Type	dp		dl		ci		rp		ap	
	w.r.	glass	w.r.	glass	w.r.	glass	w.r.	glass	w.r.	glass
SiO_2	64.3	74.1	66.1	73.1	58.4	73.5	66.4	71.2	60.6	67.4
TiO_2	0.64	0.16	0.58	0.06	0.90	0.10	0.46	0.19	0.81	0.63
Al_2O_3	15.2	11.6	15.5	11.5	16.7	11.2	15.3	13.3	16.0	13.9
Fe_2O_3 total	4.42	0.35	4.03	0.57	6.62	0.73	3.07	1.20	5.78	2.99
MnO	0.07	0.04	0.07	0.05	0.11	0.02	0.08	0.06	0.09	0.05
MgO	1.94	0.10	1.73	0.03	2.97	0.02	0.90	0.30	2.98	0.85
CaO	4.19	0.75	3.79	0.48	5.60	0.56	3.25	1.45	5.46	2.94
K_2O	3.12	5.31	3.48	4.64	2.84	4.66	3.18	3.42	2.49	3.42
Na_2O	2.94	2.68	3.11	3.74	3.26	3.20	3.54	3.40	3.16	4.02
P_2O_5	0.17	0.03	0.14	b.d.	0.24	0.11	0.18	0.03	0.18	0.11
H_2O	1.66	2.68	1.17	2.84	1.84	3.30	3.21	2.64	1.90	1.26
CO_2	0.07	–	0.05	–	0.06	–	0.13	–	0.06	–
Total	98.70	97.80	99.74	97.00	99.60	97.45	99.68	97.28	99.57	97.63
Rb	172	252	176	203	156	–	121	109	105	144
Sr	323	79	285	57	357	–	362	169	339	195
Y	17	9	18	5	22	–	23	18	22	25
Zr	140	76	137	47	168	–	211	102	146	201
Nb	12	10	14	5	14	–	13	9	12	9
Ba	474	348	456	195	481	–	752	557	431	504
La	30	29	33	16	34	–	32	25	27	27
Ce	61	51	64	23	72	–	60	51	55	59
Nd	25	–	26	–	33	–	29	–	25	–
Sm	4.8	–	5.0	–	6.8	–	6.0	–	4.9	–
Eu	0.98	0.9	0.99	0.6	1.4	–	1.2	2.3	1.1	1.5
Th	20	30	24	21	18	–	9.0	9	13	13
U	8.5	13	9.9	8	7.3	–	2.6	2	4.7	7
$^{87}Sr/^{86}Sr$	0.708670		–	–	0.708545		0.709008		0.708913	
$^{143}Nd/^{144}Nd$	0.512270		–	–	0.512280		0.512273		0.512294	

74 wt% (Fig. 3). Andesitic pumices from the LPI II unit have SiO_2 contents between 60 and 62 wt% (Fig. 3). Most dacitic pumices of LPI I and LPI II plot in a narrow range between 65 and 67 wt% SiO_2, which is similar to the typical large-volume APVC ignimbrites (65–70 wt% SiO_2). Rare quartz-free dacitic pumices from the upper LPI II unit fall between the fields defined by the andesitic and dacitic pumices in Fig. 3. The most evolved pumices in the Purico units are from the LPI II fall deposit and the lowermost part of the overlying flow, and these show a variation in SiO_2 between 68 and 74 wt%. Although not all of these pumices are rhyolites in the strict sense (> 70 wt% SiO_2) we will hereafter refer to them as rhyolite or rhyolitic for convenience.

The variations in major elements with increasing SiO_2 (decreasing total Fe_2O_3, CaO, TiO_2, MgO, MnO, and increasing K_2O) are consistent with progressive fractionation of observed phenocryst phases, in particular plagioclase, orthopyroxene, clinopyroxene, and/or hornblende. However, the concept of a continuous fractionation series from andesite to rhyolite is at odds with the trace element data (Fig. 3), which show divergent compositional trends for the different pumice types. For example, the variation trends of Sr and Rb from andesite and rhyolite are steeper than those within the dacite samples, suggesting that fractionation was governed by different bulk mineral-melt distribution coefficients (D), i.e., higher D_{Sr} in the dacites for a given D_{Rb}. This contrast is more prominent in the case of Ba and Zr, which show enrichment with increasing SiO_2 in the rhyolites, but depletion in the dacites (Fig. 3). Depletion in the dacites suggest that the melts were saturated in biotite and/or K-feldspar (for Ba) and zircon (for Zr). If the rhyolites were derived from continued fractionation of the dacite magma, it is difficult to understand why Ba and Zr depletion did not continue in the rhyolites. Furthermore, the contents of Th and U, both highly incompatible trace elements, are exceptionally low in the rhyolite compared with the dacite and andesite, although the Th/U ratios remain constant (~3) for the whole compositional range. The rhyolites cannot therefore be simply related to the dacites by fractional crystallization.

Figure 4 shows the REE abundance patterns in the pumices, and for comparison, a basaltic andesite (mafic inclusion) from one of the younger domes. The REE patterns are moderately steep for all pumice types, with La/Yb_n between 8 and 13, and they steepen progressively with fractionation from basaltic andesite ($La/Yb_n = 4.0$) to andesitic ($La/Yb_n = 8.3$) and to the dacitic

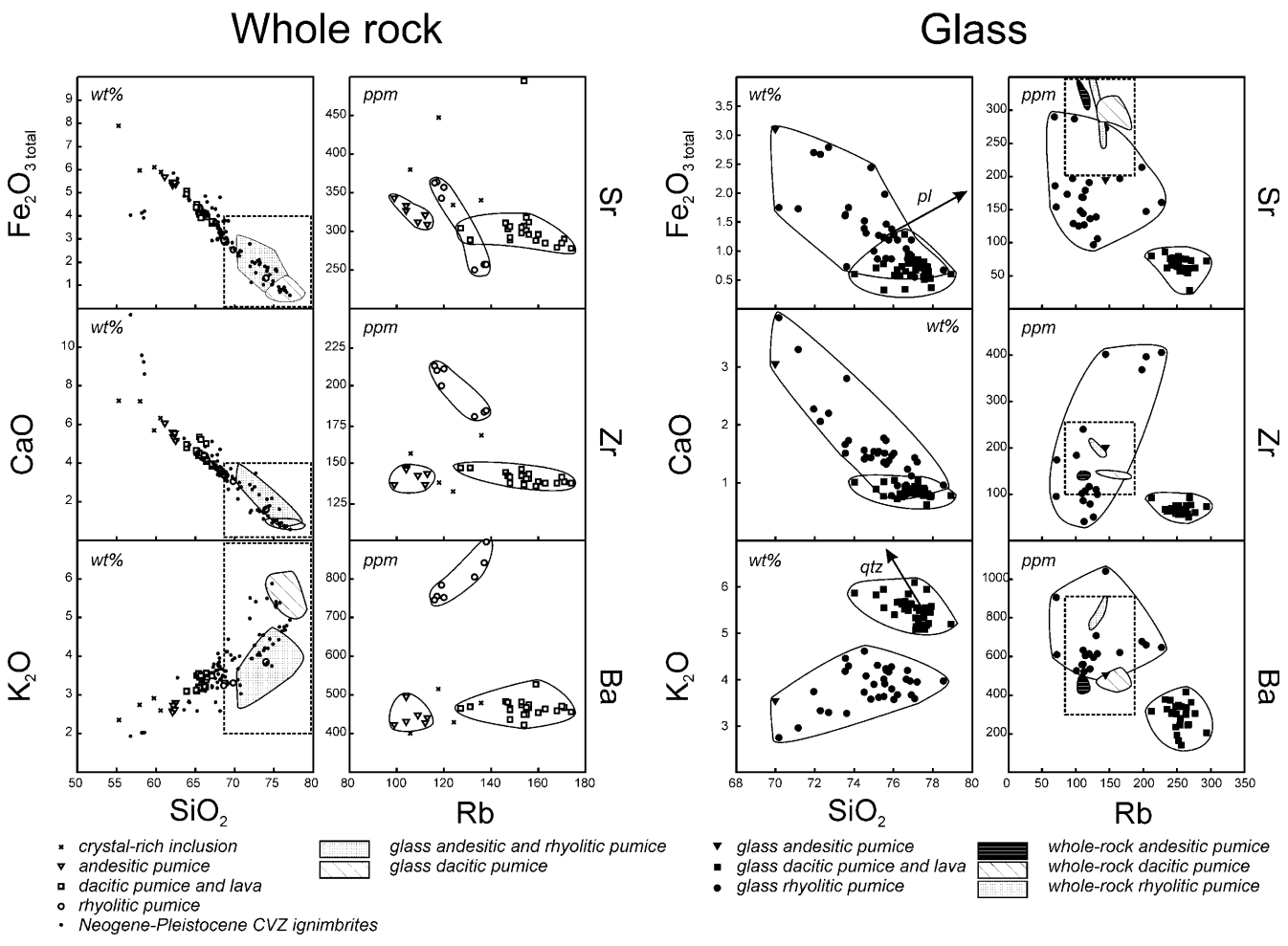

Fig. 3 SiO_2 and Rb versus selected major and trace elements of Purico whole rock samples (*left*) and LPI glasses (*right*). *Small dots* represent the compositional range of APVC ignimbrites between 22 and 24°S (Schmitt 1999). Trends for host-mineral crystallization of melt inclusions are indicated by *arrows*. Note that major element variations indicate negligible post-entrapment crystallization

pumices ($La/Yb_n = 12.3$). This steepening correlates with an increase in the negative Eu anomaly (decreasing Eu/Eu* from 0.75 to 0.67). Again, the relatively flat pattern of rhyolitic samples ($La/Yb_n = 9.3$) and relatively low Eu/Eu* ratio of ~0.7 are inconsistent with the rhyolites being a continuation of the andesite–dacite trend.

The initial Nd and Sr isotopic compositions (calculated for 1.3 Ma) of representative pumice samples including andesites, dacites, and rhyolites are indistinguishable within the range of error ($\epsilon Nd = -6.7$ to -7.2 and $^{87}Sr/^{86}Sr = 0.7085$ to 0.7090 resp.; see Table 2 and Fig. 5). The overlap of isotopic ratios with the range of basement compositions (e.g., Lucassen et al. 1999) is the most widely cited evidence for a crustal source of the APVC magmas (Hawkesworth et al. 1982; de Silva 1991) and is discussed in greater detail in a later section. Published $^{87}Sr/^{86}Sr$ ratios for the young Chascon–Aspero domes are between 0.707 and 0.709, slightly lower than the Purico ignimbrite values. Mafic inclusions in the dome lavas have the least radiogenic Sr ratios ($^{87}Sr/^{86}Sr = 0.706$) and the highest ϵNd values (–3.2) of all Purico–Chascon–Aspero samples, which has been explained by a greater proportion of mantle-derived components in the younger domes (Hawkesworth et al. 1982; Davidson et al. 1990).

In summary, the whole-rock geochemical and isotope data show that the Purico magmas cover the composi-

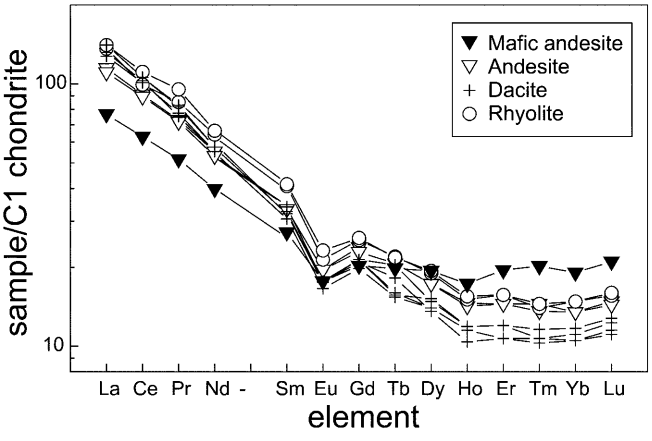

Fig. 4 C1 chondrite-normalized (Anders and Grevesse 1989) REE patterns for Purico pumices and lavas. Mafic andesite is an olivine-bearing inclusion in Chascon dacite lava and is shown for comparison

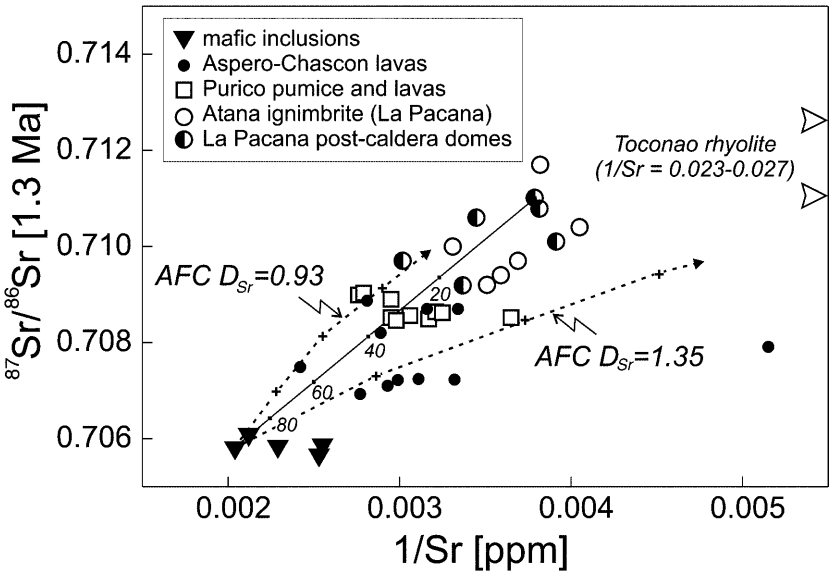

Fig. 5 Initial Sr isotopic compositions versus Sr abundance in Purico ignimbrites and lavas including Purico, Chascon and Aspero data from Hawkesworth et al. (1982) and de Silva (1991). For comparison, values for ignimbrites and post-caldera domes ranging in age from 4.1–2.6 Ma of the nearby La Pacana system are plotted (data from Lindsay 1999). Mixing line (*solid*) and assimilation-fractional crystallization (AFC) lines (*dashed*) were calculated for dacitic post-caldera dome (Cerro Bola from La Pacana) and basaltic–andesite inclusion in Chascon–Aspero lavas as end-members. +10% steps in fraction of remaining melt. Ratio of assimilation to crystallization rate in AFC model = 0.8. *Numbers* indicate mixing proportions in percent

tional range of typical large-volume ignimbrites from the APVC province. The variation in chemical composition with stratigraphic position in the Purico ignimbrites indicates that the Purico magma chamber was compositionally zoned at the time of LPI II eruption, but the concept of a regular differentiation from the least evolved andesite through dacite to the most evolved rhyolite is not supported by the data. Despite its minor volume, the rhyolite is clearly part of the Purico magma system and the issue of its origin is essential to understand how this system evolved.

Mineral chemistry and the composition of matrix and melt inclusion glasses

Methods

The melt inclusions analyzed are sufficiently large (> 50 μm in diameter) to represent true liquid compositions (Roedder 1984; Lu et al. 1995), and the effects of local compositional gradients in the melt (e.g., boundary layer effects at the crystal surface) and post-entrapment changes (e.g., crystallization of the inclusion host) can be neglected (see below). Cracked inclusions and inclusions with daughter crystals or large bubbles (> 5 vol% of the inclusion volume) were avoided. Melt inclusions from LPI II were generally pristine (undevitrified) whereas quartz-hosted inclusions of LPI I had to be rehomogenized by heating prior to analysis. Since quartz is lacking in the rhyolites, only plagioclase-hosted inclusions could be studied. Mineral compositions were determined to provide constraints on intensive parameters of crystallization and empirical mineral-melt distribution coefficients were obtained by trace element analysis of mineral and matrix glass pairs from individual pumice clasts (see Appendix for analytical details).

Mineral compositions

Plagioclase is generally the most abundant phenocryst phase in all pumice and lava types. Photomicrographs, compositional ranges and profiles of selected phenocrysts from the Purico dacite and rhyolite are presented in Figs. 6, 7 and 8. The compositional range in the LPI I dacite (An_{38}–An_{48}) is more restricted that in the LPI II dacite pumice (An_{38}–An_{68}). On average, plagioclase phenocrysts from rhyolitic pumice (An_{40}) are slightly less calcic than those from dacitic pumice as might be expected, but some cores of normally-zoned plagioclase from the rhyolite have highly calcic compositions (maximum An_{80}), which are in the range displayed by plagioclase phenocrysts in the andesitic pumice (An_{70}–An_{80}). The andesite plagioclase commonly displays sieve textures, with cores intensely infiltrated by blebs of matrix glass. Clear rims and groundmass plagioclase from the andesite are less anorthitic (An_{60}). The UPI dacite pumices contain oscillatory zoned plagioclase with high-An cores ($\sim An_{80}$) locally preserved, and with compositions from phenocryst rims and matrix microlites (An_{42}–An_{67}) in the same range as the LPI dacites. Plagioclase phenocrysts from Dome D and Chascon-Aspero dacite lavas show no obvious textural or compositional differences from the dacite pumices. The mafic inclusions in the younger domes typically have high-An plagioclase laths in the groundmass (An_{74}–An_{83}).

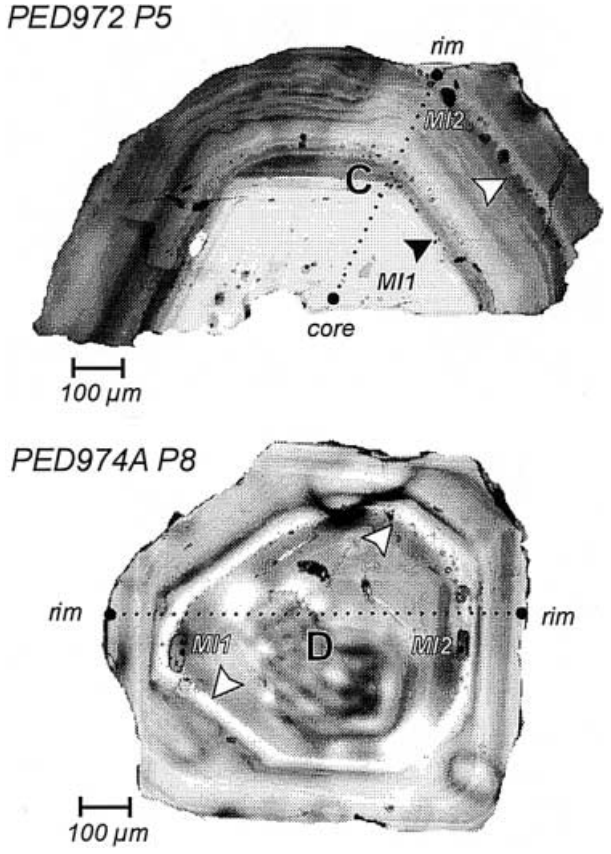

Fig. 6 Photomicrographs (cross-polarized light, analyzator in) of plagioclase phenocrysts in rhyolitic pumice from LPI II. *Arrows* indicate former dissolution surfaces. Note glassy melt inclusions aligned on euhedral growth zones. Positions of microprobe and SIMS traverses from Fig. 8C, D are indicated

Oscillatory zoned euhedral plagioclase from the LPI I and LPI II dacites revealed only minor variation in anorthite content within the cores and the near-rim areas in (generally <10 mol% An). Sr and Ba contents in individual phenocrysts are uniform within the analytical error. In contrast, plagioclase phenocrysts from the rhyolite have more complex zonation patterns and a wider range in An (35 mol%), Sr (800–1,100 ppm) and Ba (210–340 ppm). Truncations of oscillatory growth zones correlate with abrupt shifts in composition (up to 17 mol% in An content, see Figs. 6 and 7) and these indicate former dissolution surfaces. The rim compositions of the overgrowth zones are typically $\sim An_{40}$. Sr and Ba correlate negatively with An contents, and low-Ca plagioclase in the rhyolite has the highest Sr abundance (Sr = 1,100 ppm, Ba = 340 ppm).

Amphibole and magnesian biotite (mg# = 65) are the most abundant mafic minerals in the dacite pumice, lavas, and crystal-rich inclusions (Table 3). Amphibole compositions range from magnesian hornblende to magnesian edenite (mg# = 60–70). The rhyolitic pumice contains rare magnesian pargasite (mg# = 67). Opacitic rims consisting of fine-grained oxides and pyroxene (analysis see Table 4) were found only in the UPI unit.

Minor orthopyroxene (hypersthene with average mg# = 64) is present in dacite pumice from the upper portion of LPI II, in UPI and in dome lavas (Table 4), and it occurs both as single phenocrysts and fine-grained clots intergrown with Fe–Ti oxides. Commonly, orthopyroxene is partially mantled by reaction rims of hornblende, but orthopyroxene has also been observed to mantle biotite in the quartz-free LPI II dacitic pumice. The andesites contain abundant orthopyroxene (mg# = 68)

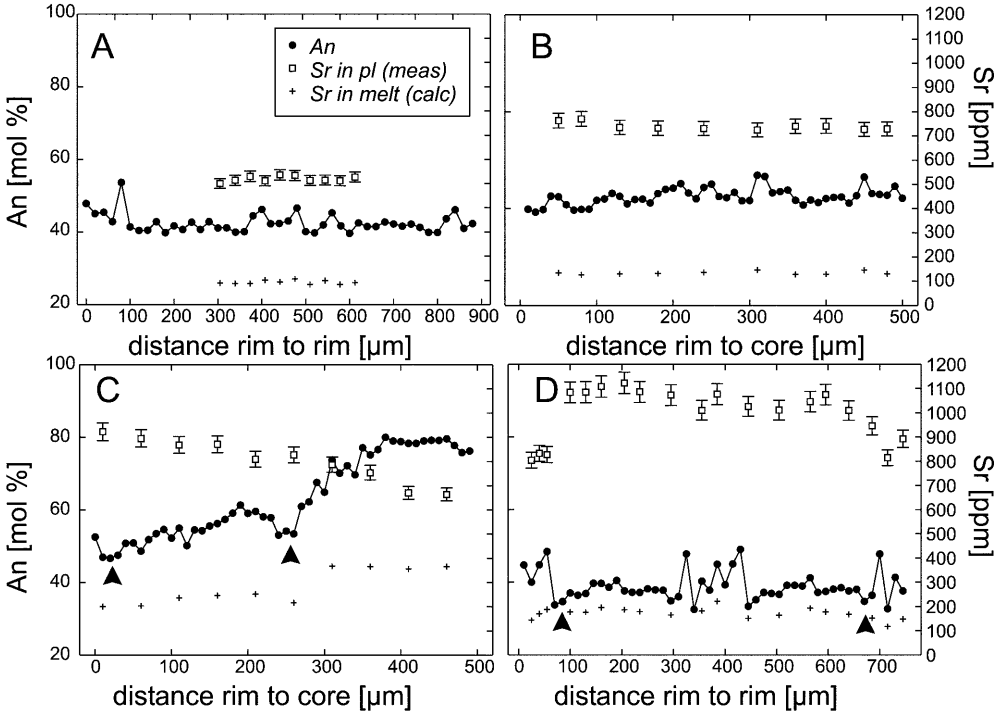

Fig. 7 Examples of zonation profiles of plagioclase phenocrysts from dacitic (**A** and **B**) and rhyolitic (**C** and **D**) pumice. Sr concentration in melt were calculated from mineral-melt partitioning according to Blundy and Wood (1991) at temperatures of 800 and 850 °C for the dacite and rhyolite, respectively

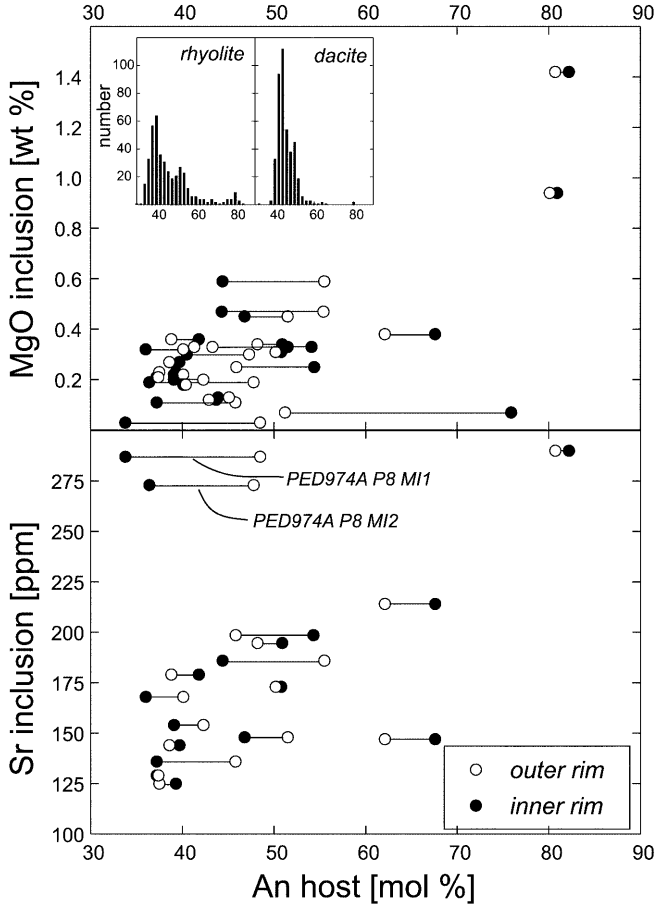

Fig. 8 MgO and Sr in melt inclusions from LPI II rhyolitic pumice versus An contents of the adjacent host plagioclase. *Insert* compares average and range in An composition from microprobe traverses of plagioclase phenocrysts of LPI II rhyolitic and dacitic pumice (~20 phenocrysts analyzed each)

and augitic clinopyroxene (mg# = 74) as the only mafic phases, and both are uniform in composition (Table 4).

Magnetite and minor ilmenite are present in all pumice types (Table 5). The Fe–Ti oxide grains generally lack exsolution lamellae, which is a prerequisite for applying two-oxide thermometry (see below). Sanidine is absent in the Purico units although it has been found as a minor constituent in some compositionally similar APVC dacitic ignimbrites (e.g., Atana and Tara ignimbrites; Lindsay et al. 2000) and domes (e.g., Cerro Chao; de Silva et al. 1994; Chason-Runtu Jarita; Watts et al. 1999).

Matrix and melt inclusion glasses

Using SiO_2 as a fractionation index, the matrix glasses from the andesitic pumice are the least fractionated (SiO_2~70 wt%), followed by rhyolitic pumice (SiO_2 = 74–77 wt%) and dacite pumice (SiO_2 = 77–78 wt%). The andesite matrix glass has the highest total Fe_2O_3 (~3.2 wt%), CaO (~3 wt%) and MgO (~0.9 wt%) of all Purico glasses, these elements being strongly depleted in the dacite pumice glasses (Fig. 3). Matrix glasses from the crystal-rich inclusions and Dome D lavas have compositions similar to those of the dacite pumice glass, which indicates that the variations observed in whole-rock compositions in this case result from variations in composition and modal abundance of phenocrysts. The glass in dark parts of the banded pumices is compositionally identical to the matrix glasses of the andesite, and glass from the light parts resembles the dacite matrix glass, indicating that the magma mingling in the banded pumice involved little or no chemical interaction.

Petrographic details and compositions of quartz- and plagioclase-hosted melt inclusions are summarized in Table 6 and Table 2 in the electronic supplementary material. In general, quartz is the more stable host for melt inclusions, but plagioclase has the advantage that the inclusions can be correlated with petrographic and chemical features of the host (zoning) and, in any case, quartz phenocrysts are lacking in the rhyolite.

For the Purico rhyolite, we distinguished two types of melt inclusions:

1. Irregularly distributed, generally small (< 30 μm) inclusions are common in high-An cores. These inclusions presumably originated from resorption of the host mineral and subsequent annealing of melt pockets. Only minor compositional shifts in the host plagioclase are found around these inclusions (Fig. 8).

2. Large inclusions (up to 75 μm in length) aligned parallel to crystallographic growth planes that were apparently trapped during periods of rapid crystal growth. Reversals in An content of the host are commonly associated with the inclusion-rich zones (Figs. 7 and 8).

Variations in glass compositions in terms of selected major and trace elements against SiO_2 and Rb were shown along with whole-rock data in Fig. 3. Major compositional changes caused by post-entrapment crystallization of the inclusions can be ruled out because the observed variations do not correlate with calculated trends for host-mineral crystallization. A comparison of glass compositions from the distinct pumice types shows the following important points:

1. Trace element abundances underscore the whole-rock evidence for divergent trends between dacitic and rhyolitic pumice. Matrix and melt inclusion glasses from the rhyolite have relatively high compatible trace element abundances (e.g., Sr = 150–290 ppm), whereas glasses in the dacites have a lower and more narrow range in Sr, averaging 70 ± 20 ppm.

2. Ba and Zr in dacite and rhyolite glasses define distinct populations (Fig. 3). Compared with whole-rock compositions, Ba and Zr in glasses are enriched or only moderately depleted in the rhyolite, whereas both are strongly depleted in the dacite.

3. Melt inclusions from Ca-rich cores in rhyolite plagioclase have very low incompatible trace element concentrations (e.g., Rb = 72 ppm, Th = 7 ppm). These abundances are even lower than in the matrix glass of andesitic pumice (Rb = 144 ppm, Th = 13 ppm).

Table 3 Selected microprobe analyses of amphibole and biotite. *dp* Dacitic pumice; *dl* dacitic lava; *ci* crystal-rich inclusion; *rp* rhyolitic pumice; *ap* andesitic pumice; *mi* mafic inclusion. Oxides in wt%; FeO and Fe_2O_3 for amphibole based on minimum ferric Fe estimate for 15 cations excluding (Na + K)A after Schumacher (1997). Temperatures calculated according to the plagioclase–edenite–richterite exchange equilibrium of Holland and Blundy (1994) using average An content of plagioclase rims at a pressure of 200 MPa (±40 °C error). Pressure estimated by Al-in-hornblende barometry, corrected for temperature derived from Fe–Ti-oxide thermometry using equations in Anderson and Smith (1995). Error in Al-in-hornblende barometry calibration ±50–60 MPa (Anderson and Smith 1995), cumulative errors of Al determination and temperature correction ±50 MPa

Sample	ZAP9616	SIL963	PED979	PED9728	PED972	PED9714	CHA974	CHA973	ZAP9616	PED976
Unit	dp	dp	dl	ci	rp	dt	dl	mi	dp	rp
Type	LPI I	LPI I	dome D	LPI II	LPI II	UPI	Chascon	Chascon	LPI I	LPI II
Mineral	Mg-ed	Mg-hbl	Mg-ed	Mg-hbl	Mg-parg	Mg-ed	Mg-parg	Mg-parg	bio	bio
SiO_2	46.27	47.25	45.19	47.70	41.68	48.02	43.46	44.27	37.87	36.07
TiO_2	1.50	1.49	1.74	1.34	2.97	1.76	1.51	1.95	4.97	3.86
Al_2O_3	7.41	7.33	8.86	6.83	12.67	7.73	12.05	12.32	14.11	15.03
FeO total	13.85	13.36	14.67	12.43	12.64	13.03	11.90	11.99	15.57	15.03
FeO	10.93	10.97	12.99	10.28	10.68	12.56	10.08	8.51	–	–
Fe_2O_3	3.25	2.66	1.86	2.39	2.18	0.18	2.01	3.88	–	–
MnO	0.41	0.49	0.42	0.39	0.19	0.31	0.23	0.16	0.13	0.22
MgO	14.21	14.43	12.98	14.48	13.31	14.79	14.82	15.20	14.56	14.60
CaO	11.46	11.95	11.58	12.56	11.47	11.55	11.13	11.66	b.d.	0.21
Na_2O	1.18	1.17	1.29	1.06	2.08	1.31	2.41	2.11	0.11	0.56
K_2O	0.84	0.78	1.09	0.64	0.62	0.71	0.72	0.60	9.19	8.62
P_2O_5	b.d.	0.05	0.01	0.01	0.05	0.03	0.03	b.d.	b.d.	b.d.
F	0.36	0.03	0.09	0.20	0.24	0.18	0.89	b.d.	0.03	0.67
Cl	0.10	0.11	0.13	0.07	0.03	0.08	0.03	0.01	0.15	0.07
–O = F	−0.15	−0.01	−0.04	−0.09	−0.10	−0.08	−0.38	–	−0.01	−0.28
–O = Cl	−0.02	−0.02	−0.03	−0.02	−0.01	−0.02	−0.01	–	−0.03	−0.02
Total	97.74	98.68	98.17	97.84	98.05	99.12	98.98	100.66	96.63	94.63
	An_{45}	An_{45}	An_{45}	An_{45}	An_{40}	An_{45}	An_{40}	An_{65}		
T (°C)	795	800	800	730	835	800	830	890		
P (MPa)	160	150	270	120	–	–	–	–		

Table 4 Selected microprobe analyses of pyroxene phenocrysts and thermometry results. *dp* Dacitic pumice; *dl* dacitic lava; *dt* dacitic tuff; *rp* rhyolitic pumice; *ap* andesitic pumice. Oxides in wt%; FeO and Fe_2O_3 calculated by stoichiometric criteria after Droop (1987). Temperatures calculated for cpx and opx pairs using the QUILF program of Andersen et al. (1993) with uncertainties for T of ∼±50 °C

Sample	SIL963	PED979	PED976	PED9721A	PED9721A	PED962A	PED962A	PED9714	PED9714	CHA973
Unit	LPI I	dome D	LPI II	LPI II	LPI II	LPI II	LPI II	UPI	UPI	Chascon
Type	dp	dl	rp	ap	ap	ap	ap	dt	dt	dl
Mineral	opx	opx	opx	opx	cpx	opx	cpx	opx	cpx	opx
SiO_2	55.28	52.17	51.90	54.03	51.20	53.45	51.24	53.21	52.69	51.84
TiO_2	0.23	0.32	0.24	0.16	0.40	0.27	0.46	0.14	0.73	0.36
Al_2O_3	2.62	1.47	2.62	0.73	2.25	1.03	1.73	0.82	4.43	3.06
FeO total	11.31	21.07	16.95	19.84	9.65	17.42	9.28	20.98	12.48	5.53
FeO	11.22	20.91	14.90	19.84	9.65	17.42	8.54	20.72	12.48	5.65
Fe_2O_3	0.10	0.18	2.29	–	–	–	0.82	0.29	–	–
MnO	0.22	0.70	0.36	0.78	0.29	0.51	0.30	0.70	0.21	0.00
MgO	29.67	22.19	24.48	23.79	13.38	24.99	14.97	23.17	18.28	15.87
CaO	1.25	1.14	2.52	0.87	20.70	1.21	20.45	0.80	11.09	22.37
Na_2O	0.03	0.02	0.07	0.03	0.38	0.02	0.30	0.02	0.55	0.22
Total	100.62	99.10	99.37	100.24	98.24	98.89	98.82	99.83	100.46	99.25
T [°C]				880		965		825		

4. Melt inclusion compositions in the rhyolite become more evolved (e.g., decreasing MgO and Sr contents) with decreasing An content of the adjacent host plagioclase, indicating that the melt composition changed during crystallization and trapping (Fig. 8). In contrast, quartz- and plagioclase-hosted inclusions from the dacite are homogeneous and similar to matrix glass composition.

Distribution coefficients

Empirical mineral-melt partition coefficients for plagioclase, amphibole, and biotite in dacitic pumice were derived from trace element compositions in phenocrysts and matrix glasses determined by SIMS and LA-ICP-MS analysis. The calculated D values are given in Table 7 and the data are available in the electronic supplemen-

Table 5 Selected microprobe analyses and thermometry results of magnetite–ilmenite pairs. *dp* Dacitic pumice; *rp* rhyolitic pumice; *ap* andesitic pumice; *dl* dacitic lava. Oxides in wt%; FeO and Fe_2O_3 calculated by stoichiometric criteria after Droop (1987). Temperatures and oxygen fugacities calculated using the QUILF program of Andersen et al. (1993) with quoted uncertainties for T of $\sim \pm 25$ °C and 0.3 log units for fO_2 given an uncertainty of 1 mol% for the ilmenite and magnetite composition by electron microprobe analysis

Sample	PED971		PED962H		PED972		PED962B		PED979		CHA974	
Unit	LPI I		LPI II		LPI II		LPI II		dome D		Chascon	
Type	dp		dp		rp		ap		dl		dl	
Mineral	Ti-Mag	Ilm	Ti-Mag	Ilm	Ti-Mag	Ilm	Ti-Mag	Ilm	Ti-Mag	Ilm	Ti-Mag	Ilm
SiO_2	0.09	b.d.	0.05	0.03	0.04	0.03	0.07	0.04	0.09	b.d.	0.05	0.79
TiO_2	6.29	42.39	1.72	42.30	5.57	30.32	10.56	39.96	6.41	42.11	4.39	37.22
Al_2O_3	2.00	0.49	7.06	0.05	2.68	0.63	2.82	0.19	2.10	0.29	1.94	0.78
Cr_2O_3	0.11	0.02	0.10	0.07	0.03	0.02	0.23	0.07	0.13	0.04	0.16	0.05
FeO total	83.00	51.29	82.42	51.96	82.84	63.01	78.11	52.37	83.80	53.06	86.06	56.74
MnO	0.62	1.05	0.91	1.03	0.67	0.37	0.33	0.30	0.64	0.86	0.38	0.59
MgO	0.91	1.74	1.30	2.03	1.40	1.24	2.50	3.33	1.11	1.67	0.73	1.56
FeO	34.68	33.87	33.68	33.35	33.45	24.68	36.78	29.55	34.91	33.95	33.68	30.90
Fe_2O_3	53.78	19.38	54.25	20.72	54.97	42.66	46.01	25.40	54.42	21.27	58.30	28.76
Total	98.48	98.94	98.48	99.58	98.85	99.96	99.28	98.93	99.81	100.23	99.66	100.65
T (°C)	780		773		850		885		785		770	
log fO_2	−12.7		−12.7		−10.6		−10.8		−12.4		−12.1	

tary material (Table 3). Comparison with literature data for similar compositions (e.g., dacite from Ewart and Griffin 1994) shows generally good agreement with values determined in our study.

Pre-eruptive magma conditions

Mineral thermometry and barometry

Magmatic temperatures were derived using the Fe–Ti-oxide thermometer (Andersen and Lindsley 1988; Andersen et al. 1993), the plagioclase–amphibole thermometer (Holland and Blundy 1994) and two-pyroxene geothermometry (Lindsley 1983; Andersen et al. 1993).

Fe–Ti oxide thermometry was based on at least five magnetite and ilmenite pairs from each sample. All samples met the criterion for equilibrium based on the systematic Mn and Mg partitioning in the oxide phases (Bacon and Hirschmann 1988) and no difference was found between touching mineral pairs and isolated phenocrysts. Fe–Ti-oxide temperatures for the quartz-bearing dacite pumices, crystal-rich inclusions, a tuff sample from UPI, two Dome D lavas and one Chascon lava range from 750–800 °C. Temperatures obtained from andesitic pumice are higher, at 860–880 °C. Most oxide pairs in the rhyolite record similarly high temperatures ~850 °C and the total range is 800–870 °C. Oxygen fugacities calculated from the data are generally 1.5 log units above the Ni–NiO-buffer.

Plagioclase and amphibole rim compositions from the dacite pumice yielded edenite–richterite exchange temperatures between 750 and 810 °C, calculated for pressures between 100 and 300 MPa based on Al-in-hornblende barometry (see below). Coexisting plagioclase and amphibole in rhyolitic pumice yield higher temperatures between 840 and 880 °C. These results are in good agreement with Fe–Ti-oxide temperatures from both groups of samples. The plagioclase–amphibole temperatures from Chascon lavas and inclusions (830–890 °C) are slightly higher than the corresponding Fe–Ti oxide temperatures.

Temperatures calculated from two-pyroxene thermometry for the andesites (965 °C) exceed the corresponding Fe–Ti-oxide temperatures. Similar discrepancies between Fe–Ti-oxide and two-pyroxene geothermometry were reported for andesite lavas from Lascar volcano (Matthews et al. 1994) and this problem may reflect a higher closure temperature for the pyroxenes compared with magnetite and ilmenite.

A temperature increase of ~50 °C from dacite to rhyolite is documented by various independent geothermometers and this constitutes further evidence that the rhyolite cannot have originated by fractionation of the dacite. Given the precision of ±25 °C for Fe–Ti-oxide temperatures (Andersen et al. 1993) and ±50 °C for pyroxene thermometry (Lindsley 1983), the temperature variations indicate that the incoming andesite was at least ~100–200 °C hotter than the resident dacite. Heating of the dacite at the magma interface might explain the presence of opacitic rims in the late- erupted UPI dacite (two-pyroxene temperature: 825 °C). Heating of dacitic magma by still later recharge events could account for the high temperatures recorded in Chascon–Aspero dacite lavas.

The temperature-corrected Al-in-hornblende barometer (Anderson and Smith 1995) was applied to the LPI dacites. Application of the barometer in this case is justified despite the lack of sanidine because the melt phase has $SiO_2 > 76$ wt% and $K_2O > 5$ wt%, thus fulfilling the criteria of Johnson and Rutherford (1989). Errors in the calibration, Al-determination, and temperature correction of this barometer are considerable (at least ±60 MPa). but the pressure estimates between 110 and 220 MPa suggest that the Purico dacites equil-

Table 6 Selected analyses of plagioclase- and quartz-hosted melt inclusions. Major elements in wt% (normalized to 100%); traces in ppm; An in mol%. *dp* Dacitic pumice; *rp* rhyolitic pumice. Methods for glass analysis explained in Table 2 and Appendix

Sample	PED971 P2–1	PED971 P8–1	PED971 Q1–1	PED971 Q1–2	PED962H P2–1	PED962H P4–1	PED962H Q1–1	PED962H Q2–1	PED972 P5–1	PED972 P8–1	PED974A P8–1	PED974A P8–1
Unit	LPI I/A	LPI I/A	LPI I/A	LPI I/A	LPI II/A	LPI II/A	LPI II/A	LPI II/A	LPI II/A	LPI II/A	LPI II/A	LPI II/A
Type	dp	dp	dp	dp	dp	dp	dp	dp	rp	rp	rp	rp
Host	pl	pl	qtz	qtz	pl	pl	qtz	qtz	pl	pl	pl	pl
Remarks	Moderately devitrified	Moderately devitrified	Devitrified, heated	Devitrified, heated	Moderately devitrified	Moderately devitrified	Incipiently devitrified	Incipiently devitrified	Undevitrified	Undevitrified	Undevitrified	Undevitrified
An rim	40.5	47.4	–	–	47.0	41.6	–	–	80.7	62.1	40.1	47.8
An core	42.9	48.4	–	–	51.4	44.1	–	–	82.2	67.8	36.0	36.4
SiO_2	77.2	77.6	77.3	76.0	77.7	77.8	76.4	76.8	72.7	73.5	74.5	74.8
TiO_2	0.09	0.14	0.12	0.11	0.09	0.15	0.14	0.11	0.11	0.11	0.30	0.69
Al_2O_3	12.7	12.5	12.6	13.4	12.2	12.2	12.9	12.5	14.0	15.0	14.2	13.2
Fe_2O_3	0.77	0.81	0.78	0.58	0.73	0.65	0.73	0.93	2.79	1.61	1.52	2.44
MnO	0.05	0.01	0.01	0.11	0.03	0.03	0.02	b.d.	0.09	0.11	0.08	0.06
MgO	0.10	0.09	0.10	0.06	0.07	0.04	0.04	0.11	1.42	0.38	0.32	0.19
CaO	0.80	0.91	0.83	1.04	0.62	0.79	0.75	0.82	2.20	1.66	1.41	1.43
K_2O	5.55	5.33	5.32	5.40	5.95	5.21	5.63	5.49	3.29	4.18	4.62	3.58
Na_2O	2.80	2.62	2.94	3.28	2.64	3.05	3.33	3.31	3.17	3.36	3.05	3.44
P_2O_5	b.d.	b.d.	0.04	b.d.	b.d.	b.d.	0.01	b.d.	0.27	0.04	b.d.	b.d.
H_2O SIMS	2.5	2.1	3.8	3.9	2.8	1.5	3.4	3.3	3.2	3.6	4.6	4.0
Rb	267	294	248	252	244	242	235	263	68	198	111	137
Sr	61	72	71	71	77	66	62	56	290	214	168	272
Y	8	31	8	5	8	26	10	12	14	29	25	28
Zr	51	74	58	56	65	70	63	62	174	369	240	382
Nb	8	20	9	8	12	10	7	7	9	32	13	17
Ba	248	206	340	164	313	305	328	300	610	678	560	1058
La	21	12	27	30	26	28	24	29	20	22	23	24
Ce	40	26	43	36	41	49	44	49	42	40	49	51
Th	32	24	29	29	21	15	25	29	7	30	10	–
U	13	21	13	13	13	6	13	43	2	9	4	11

Table 7 Mineral/melt partition coefficients for Purico dacite (PED962H). *n* Number of replicate analyses. Trace element abundance in minerals determined by LA-ICP-MS, glass composition by SIMS (see Appendix for analytical procedures). *E&G* Range of partition coefficients for low-Si rhyolites and dacites from Ewart and Griffin (1994) for comparison

Mineral	Plagioclase				Hornblende				Biotite	
n (Mineral)		5			7				1	
n (Glass)		4			4				4	
	Av.	Min.	Max.	E&G	Av.	Min.	Max.	E&G		E&G
Rb	0.04	0.02	0.09	0.023–0.24	0.09	0.04	0.12	0.021–0.37	2.07	2.46–5.27
Sr	10.38	9.09	11.39	5.83–10.7	0.94	0.71	1.34	0.25–1.13	0.78	0.25–0.31
Y	0.38	0.03	1.11	0.083–0.55	16.69	14.45	18.56	4.0–45.2	0.36	0.6–2.3
Zr	0.05	0.00	0.22	0.10–0.55	1.08	0.72	1.67	0.53–0.93	0.54	0.19–0.59
Nb	0.06	0.01	0.23	0.26–0.88	1.72	1.47	1.96	1.5–6.7	2.26	4.6–>7.5
Ba	0.71	0.54	0.85	0.28–1.05	0.50	0.23	0.67	0.16–0.92	16.95	6.4–13.9
La	1.04	0.69	1.49	–	2.70	1.73	4.26	–	0.41	–
Ce	0.80	0.46	1.40	–	4.03	2.81	5.47	–	0.49	–
Eu	1.81	1.61	2.14	–	5.64	5.31	6.14	–	0.52	–
Th	0.07	0.01	0.20	–	0.15	0.08	0.26	–	0.25	–
U	0.03	0.02	0.06	–	0.08	0.04	0.12	–	0.28	–

ibrated in the upper crust (4–8 km, assuming a density of the lithostatic column of 2.7 g/cm^3).

Water contents

Pre-eruptive water contents in Purico melts have been constrained by SIMS analysis of melt inclusion glasses and by the plagioclase-melt geohygrometer of Housh and Luhr (1991). Detailed interpretation of the volatile evolution of the Purico system and other APVC felsic magmas is the subject of a separate paper and the results are only briefly summarized here (see also Schmitt and de Silva 2000).

H_2O concentration ranged from 3.5–4.2 wt% in quartz-hosted melt inclusions from dacite pumice, and from 3.2–4.8 wt% in plagioclase-hosted rhyolitic pumice. FTIR measurements showed that CO_2 contents were low (<400 ppm). The calculated water contents from plagioclase-melt equilibrium, adjusted for temperatures determined from Fe–Ti-oxide thermometry, broadly agreed with the melt inclusion data. However, for the andesite and dacite a 1 wt% difference in H_2O was found between the Ab and An calibrations of the geohygrometer, which exceeds the experimental calibration error of 0.4 wt% (Housh and Luhr 1991). No melt inclusions suitable for water determination were found in the andesitic pumice. Given the better agreement between melt inclusion data and the Ab geohygrometer calibration in the dacite samples where both methods can be compared, the Ab calibration appears preferable and this yields an estimated melt water content of ~4 wt% for the andesite, similar to that of the dacite and rhyolite magmas.

These values of melt volatile contents can be used to calculate saturation pressures if the solubilities of volatile species in melts are known. For H_2O, the melt inclusion data indicate minimum pressures between 100 and 150 MPa for both the dacite and the rhyolite, using H_2O solubility data in haplogranitic melts from Holtz and Johannes (1994). Pressure estimates for the dacite from Al-in-hornblende geobarometry are not significantly higher than the saturation pressure, suggesting that the melts may have been at saturation before eruption. The effect of CO_2 on the calculated saturation pressure, considering the very low CO_2 concentrations, is in the range of the H_2O variability in the melt inclusions.

Summary of chemical and petrologic constraints

Before discussing the broader issues of pre-eruptive zonation in the Purico magma system it is useful to reiterate our interpretation of the main results from whole-rock and phase chemistry described above:

1. Compositionally discrete magma batches were erupted from the Purico system. The isotopic similarity and constant incompatible element ratios (e.g., Th/U) over a wide compositional range of more than 10 wt% in SiO_2 suggest a common origin for all Purico magmas types, but producing the large volumes of dacite by mixing between the rhyolite and the andesite can be ruled out by volume considerations and observed trace element variations.

2. The dacite magma cannot be the precursor to the rhyolites. The compositions of the dacites are distinct from the bulk rhyolite and define different evolutionary trends. Incompatible trace elements such as Th and U are lower in the rhyolite bulk pumice and matrix glass than in the dacite. Depletion caused by partitioning into an exsolved fluid is unlikely given low fluid-melt partition coefficients for Th particularly (Keppler and Wyllie 1990). Furthermore, trends of compatible trace element variation in the andesites and rhyolites diverge from the dacites, and the rhyolites have higher equilibration temperatures. Finally, the Sr contents in the An-rich cores of plagioclase in the rhyolite require crystallization from a high-Sr melt ($\sim 380 \pm 100$ ppm, Fig. 7) according to the partitioning model of Blundy and Wood (1991). These plagioclase grains are not xenocrystic because the

Sr contents of matrix glass (~150 ppm) agree with the melt composition calculated from Sr concentration in plagioclase rims using the same method.

3. Melt inclusions in zoned plagioclase from rhyolite reveal that the trapped melt continuously changed composition during crystallization of the host and the trace element variations in the melt inclusions require a parental magma less evolved than the dacite.

4. Dissolution surfaces observed in zoned plagioclase phenocrysts in rhyolite pumice are attributed to temperature variation. Principally, changes in plagioclase An content are controlled by both temperature and water content of the melt (Housh and Luhr 1991), but in the case of volatile-saturated magmas at constant pressure, as proposed for the pre-eruptive Purico chamber, water content is buffered by H_2O solubility in the melt, and thus we believe that the dissolution surfaces indicate re-heating and not variations in H_2O (e.g., Singer et al. 1995). It should be noted that only a fraction of the phenocrysts in the rhyolite is affected. Thus, the temperature variation is likely to be a small-scale phenomenon connected with strong temperature gradients in convecting rhyolite, as opposed to external heating by new input of hot mafic melt (Singer et al. 1995).

5. Further evidence for the prevalent thermal variations in the rhyolite magma comes from melt inclusions with high Sr contents (350 ppm), trapped along a former dissolution surface in a zoned plagioclase phenocryst (Fig. 6). The zone of entrapment corresponds to an abrupt shift in An content from An_{33} to An_{50}. Neither the H_2O contents nor other chemical indices of fractionation in the inclusions (e.g., MgO, see Fig. 8) are different in the high-Sr inclusions compared with other melt inclusions in the plagioclase. Thus, plagioclase dissolution most likely resulted from a temperature increase alone and not from compositional changes in the magma. We envisage this process as taking place in a convecting rhyolitic magma with a strong temperature gradient. The high Sr contents in the melt inclusions can be explained by post-entrapment re-equilibration with host plagioclase at a higher temperature (~60 °C), causing dissolution of low-Ca (high-Sr) and precipitation of high-Ca (low-Sr) plagioclase at the inclusion wall.

6. The homogeneity of quartz- and plagioclase-hosted inclusions in the dacite and their similarity to matrix glasses suggest that the inclusions were either trapped at a late stage of magma evolution or have re-equilibrated with the surrounding melt by diffusion. The latter would imply a long residence time of the dacitic magma before eruption and a slowly cooling chamber.

Discussion

Evolution of the Purico magmatic system and origin of compositional variations

The Purico ignimbrite consists of compositionally distinct juvenile materials that have indistinguishable Nd and Sr isotopic composition. A convective fractionation mechanism (Wolff et al. 1990) has been invoked for zonation in Purico and other central Andean magma chambers by de Silva (1991). However, a combination of evidence from melt inclusion data and geothermometry indicates that the rhyolitic magma cannot be viewed simply as the evolved cap of a dacitic magma chamber as previously suggested, and a precursor more mafic than dacite is indicated.

Fractional crystallization as a mechanism of generating the observed compositional variations was tested by least-squares mixing models (LSQ) using reasonable pairs of parent and daughter melts (Tables 8, 9, and 10). Trace element variations were then modeled by the Rayleigh fractionation equation using D-values measured in the Purico dacite (Table 7) or taken from the literature for andesitic compositions (Bacon and Druitt 1988; Blundy and Wood 1991; Dunn and Sen 1994). Model 1 examines the step from andesite to dacite and the results indicate that the Purico andesite could produce dacite as a residual melt by removing plagioclase, orthopyroxene, clinopyroxene, and Fe–Ti-oxide (fraction of remaining melt $f = 0.71$). Similar f-values, between 0.65 and 0.85, were calculated for selected trace elements (Rb, Sr, Ba, and La). Small amounts of zircon fractionation (~1%) are required to explain the Y data

Table 8 Results of major element mixing models (LSQ) and trace element Rayleigh fractionation modeling. f Fraction of melt remaining. ΣR^2 Sum of squared residuals. Mineral-melt partition coefficients for andesite from Bacon and Druitt (1988), Dunn and Sen (1994) and Blundy and Wood (1991)

Model 1	Parent	Daughter	% Fractionated mineral phase						
	Andesite	Dacite	Pl An_{70} 61.9	Cpx 10.6	Opx 19.9	Mag 7.5		F 0.71	ΣR^2 0.06
	c_o	c_l	Mineral/melt partition coefficient k_D				Bulk-D		
Rb	103	156	0.16	0.03	0.01	0.01	0.10	0.63	
Sr	352	312	2.2	0.5	0.01	0.01	1.43	0.76	
Ba	423	474	0.2	0.1	0.1	0.01	0.16	0.52	
La	26	30	0.18	0.28	0.26	0.01	0.19	0.84	
Y	22	16	0.066	2.4	0.19	0.2	2.35[a]	0.79	

[a] Assumes 1% zircon in fractionating assemblage (k_D zfor Y in zircon ≈200)

Table 9 Results of major element mixing models (LSQ) and trace element Rayleigh fractionation modeling. f Fraction of melt remaining. ΣR^2 Sum of squared residuals. Mineral-melt partition coefficients for dacite from Table 7 and from Bacon and Druitt (1988), and Dunn and Sen (1994)

Model 2	Parent	Daughter	% Fractionated mineral phase						
	Quartz-poor Dacite	Dacite lava	Pl An_{50}	Hbl	Bt	Mag		F	ΣR^2
			50.5	39.2	5.2	5.2		0.80	0.24
	c_o	c_l	Mineral/melt partition coefficient k_D				Bulk-D		
Rb	126	176	0.04	0.09	2.07	0.01	0.16	0.67	
Sr	313	285	10.4	0.94	0.78	0.01	5.65	0.98	
Ba	465	456	0.71	0.5	17.0	0.01	1.43	0.96	
Y	18	18	0.38	16.7	0.36	0.2	6.76	1.00	

Table 10 Results of major element mixing models (LSQ) and trace element Rayleigh fractionation modeling. f Fraction of melt remaining. ΣR^2 Sum of squared residuals. Mineral-melt partition coefficients for andesite from Bacon and Druitt (1988), Dunn and Sen (1994) and Blundy and Wood (1991)

Model 3	Parent	Daughter	% Fractionated mineral phase						
	Andesite	Rhyolite	Pl An_{80}	Cpx	Opx	Mag		F	ΣR^2
			51.8	13.3	25.6	9.2		0.69	0.15
	c_o	c_l	Mineral/melt partition coefficient k_D				Bulk-D		
Rb	103	117	0.16	0.03	0.01	0.01	0.09	0.87	
Sr	352	362	2.2	0.5	0.01	0.01	0.95	0.56	
Ba	423	755	0.14	0.1	0.1	0.01	0.11	0.52	
La	26	33	0.18	0.28	0.26	0.01	0.20	0.74	
Y	22	25	0.066	2.4	0.19	0.2	0.42	0.79	

and are consistent with the increasing steepness of REE patterns from andesite to dacite. The variation between the least-evolved dacite pumice and evolved dacite lava from Dome D is treated in model 2. The model indicates that less fractionation is required ($f = 0.67$–0.98) and the calculated crystallizing assemblage resembles that of the crystal-rich aggregates in the ignimbrites, suggesting that they may be related to this process. Model 3 examines the possible derivation of rhyolite from a parental andesite, and illustrates that clinopyroxene and orthopyroxene-dominated fractionation ($f = 0.52$–0.85) could yield the Purico rhyolite. In support of this model, we note that the bulk rhyolite composition resembles that of matrix glass from andesitic pumice (major elements and especially Zr in Fig. 3) and that the crystallinity of the andesite (37–56%) is similar to the modeled degree of fractionation. However, the andesite matrix glasses differ from bulk rhyolite in their relatively high Rb and Th, and low Ba contents. These differences could result from disequilibrium between melt and phenocrysts in the andesite as indicated by, e.g., sieve plagioclase, and/or from mixing with the dacite magma. In other words, the composition of interstitial melt in andesite clasts that was quenched during eruption may differ significantly from the residual melt composition produced by fractionation of andesite at greater depths in the chamber. The latter may be better represented by the composition of melt inclusions preserved in high-An plagioclase cores from rhyolitic pumice (Fig. 8).

Therefore, fractional crystallization models broadly satisfy the observed chemical variations in the dacite and the transition from andesite to dacite, and andesite to rhyolite suites. The inferred changes in the fractionating assemblage are mainly temperature controlled. For example, fractionation within the cooler dacites involved biotite, zircon, and less calcic plagioclase, which resulted in depletion of the remaining melt in Zr and Ba. The absence of these phases during higher temperature fractionation of andesitic magma would cause the enrichment of Zr and Ba in the residual melt, which is required to explain the rhyolite composition.

The chemical characteristics and geothermometry data from the rhyolite suggest that its precursor magma was chemically more primitive and hotter than the Purico dacite. A mechanism capable of producing residual rhyolitic melt without prolonged fractionation and cooling is phenocryst removal from a crystal-rich magma by filter-pressing (Sisson and Bacon 1999). Rapid, buoyancy-driven ascent of the hot rhyolite magma will minimize interaction with ambient dacite in the chamber, and decompression with concomitant volatile oversaturation could lead to an overpressurization of the magma chamber sufficient to trigger eruption (e.g., Folch and Marti 1998). Figure 9 illustrates schematically our concept of how recharge of andesitic magma into a homogeneous dacite chamber produced the compositional variations of the Purico

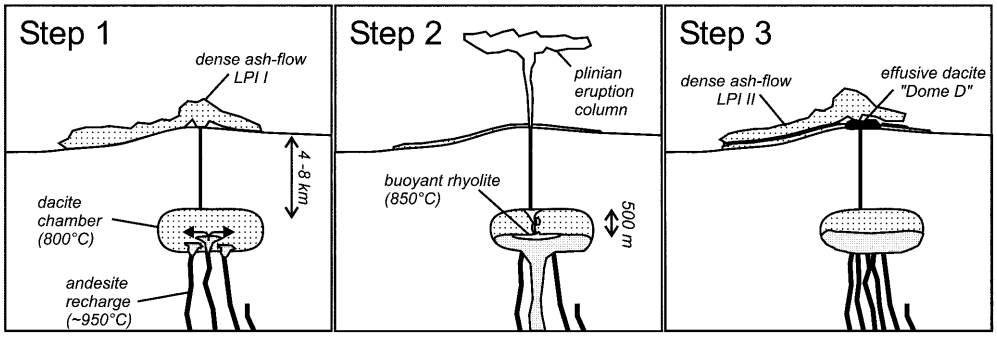

Fig. 9 Schematic evolution of the Purico magma chamber (not to scale). Step (**1**) eruption of homogeneous dacitic magma forming LPI I, perhaps triggered by andesite recharge. Step (**2**) Cooling and crystallization of injected andesite releases hot, volatile rich rhyolitic melt. Volatile exsolution during decompression leads to explosive eruption and a high temperature/high volatile magma sustains a plinian column. Step (**3**). Following the plinian eruption, the dacite and underlying andesite are subsequently tapped to form LPI II. Slowly degassed dacite magma remaining in the chamber forms late dacite-effusive domes. Magma chamber depth estimated from Al-in-hornblende barometry and minimum H_2O saturation pressures of hydrous melt (see text)

system. Following eruption of the LPI I ignimbrite, andesitic recharge led to production of a hot, volatile-rich and low-viscosity rhyolitic magma, which erupted as a sustained plinian column. Subsequent eruption of the LPI II ignimbrite progressed when entrainment of denser, volatile-poorer and more viscous magma from the main dacitic portion of the magma chamber caused the plinian eruption column to collapse. Minor volumes of reheated dacitic and andesitic magma were tapped during the waning stages of the eruption. Subsequently, degassed dacite magma was passively squeezed out by ongoing andesite ascent to form the younger dacite domes. Evidence that andesite recharge was important for the dacite dome effusion is the presence of mafic inclusions in the younger dome lavas (Hawkesworth et al. 1982; Davidson et al. 1990; Tepley and Davidson 1997).

Physical aspects and implications for styles of zonation in ignimbrites

An important question remaining is how a volumetrically minor rhyolitic melt can effectively separate from its parental magma and rise through much larger volumes of dacitic magma without mixing? This problem is not unique to the Purico system; the LPI II eruptive sequence presents a variant of the concept of silicic replenishment of intermediate magma chambers discussed by Eichelberger and Izbekov (2000) and Eichelberger et al. (2000).

Fluid dynamical experiments have shown that a low-density silicic melt injected into a resident magma tends to remain separate if viscosity contrasts are high (Campbell and Turner 1986; Huppert et al. 1986). Hot, volatile-rich and therefore less dense and less viscous rhyolitic melt released at the base of a denser, more viscous dacitic magma could rise through the latter and remain unaffected, especially if the dacite layer is thin (Huppert et al. 1984). This is all the more likely for the Purico system since the dacite magma was already partially erupted during the LPI I event. Table 11 shows calculated densities (Bottinga et al. 1982; Lange 1994; Ahrens 1995) and viscosities (Shaw 1972; Pinkerton and Stevenson 1992) of all Purico magma types. Like other studies on the viscosity of silicic magmas (Scaillet et al. 1998), we do not consider the effects of a separate volatile phase. The calculated melt viscosities differ by more than one order of magnitude, the differences mainly reflecting the temperature contrast (at least ~100 °C between andesite and dacite) rather than the different melt H_2O contents (range of ~1 wt% between dacite and rhyolite using the maximum values from melt inclusions). The effect of crystallinity on magma viscosity is also important, and Table 11 shows that the difference in magma viscosities between the crystal-rich dacite and crystal-poor rhyolite are significantly greater than the contrast in melt viscosity alone.

Experimental models of magma chamber evacuation allow an estimation of the eruption draw-up heights, which control whether or not a lower magma layer is tapped during the eruption process (Blake and Ivey 1986a, 1986b). Draw-up heights depend mainly on dis-

Table 11 Calculated pre-eruptive magma densities (crystals plus interstitial melt) and viscosities of melts and magmas of the Purico complex. Density values ρ calculated after Bottinga et al. (1982), Lange (1994) and Ahrens (1995) and viscosities η after Shaw (1972) and Pinkerton and Stevenson (1992)

Type	Crystallinity (vol%)	H_2O melt (wt%)	T (°C)	ρ magma (kg/m^3)	Logη melt (Pa s)	Logη magma (Pa s)
Andesite	40	4	900	2750	5.1	5.9
Dacite	40	4	800	2520	6.7	7.6
Rhyolite	20	5	850	2440	5.5	5.8

charge rate and the viscosity of the upper layer. The discharge rate of the Purico ignimbrite is not well constrained, but two independent estimates can be made for eruption of the basal fall deposit (following methods outlined in Carey and Sparks 1986; Wilson and Walker 1987; Carey and Sigurdsson 1989). These estimates range from 3×10^7 to 5×10^7 kg/s or 6×10^4 to 1×10^5 m^3/s, assuming a density of 500 kg/m^3, typical for most plinian eruptions (Carey and Sigurdsson 1989). Given these values and the viscosity of the dacite magma, the critical thickness of dacite which would be needed to prevent the underlying andesite magma from being tapped is between 430 and 490 m. There is no evidence that the LPI I eruption tapped andesitic magma but the andesitic clasts in LPI II ignimbrite indicate that the second eruption clearly did. This implies that the thickness of the dacite layer had decreased to a few hundred meters following the LPI I event, and therefore it seems likely that the rhyolitic melt could ascend through the dacite rapidly and with only minor cooling.

De Silva (1991) noted that compositional variation in APVC ignimbrites is greatest in the smaller deposits, whereas the large volume deposits are homogeneous. Based on these arguments of draw-up height, we can speculate that compositional zonation by mafic recharge may be a common process in the APVC magma systems generally, but it could go undetected in the larger chambers if the viscosity and thickness of the dacite layer are sufficient to prevent tapping of lower layers.

Source constraints and implications for the evolution of APVC ignimbrite volcanism

There is consensus that a large crustal contribution is present in the central Andean ignimbrite magmas, but it is unclear if the large-volume ignimbrites represent pure crustal melts (Hawkesworth et al. 1982) or products of mixing between mantle-derived mafic magmas and crustal melts (Francis et al. 1989; Ort et al. 1996). There has been very little discussion in previous studies about the depth of crustal melting or of the postulated mixing and homogenization zone. The comprehensive suite of chemical and isotopic data from the Purico complex allows us to place some constraints on the deeper roots of this magmatic system and its relationship with other, compositionally similar APVC ignimbrites. Purico is spatially associated with the La Pacana caldera complex, the largest in the APVC, and we focus on a comparison with that complex. It can be expected that the composition of the deeper sources for both will be similar despite the differences in shallow-level magma chamber evolution.

The isotopic variations within the La Pacana and Purico complexes, if considered together, show the effects of both fractional crystallization and an overall mixing or assimilation trend between a low-$^{87}Sr/^{86}Sr$ and a high-$^{87}Sr/^{86}Sr$ component (Fig. 5). The Purico suite is generally homogeneous in $^{87}Sr/^{86}Sr$ over a large range in Sr abundances, indicating a dominance of fractional crystallization versus mixing. This contrasts with the larger La Pacana complex, which displays a significant variation in Sr isotope composition, in part correlated with the degree of differentiation (Fig. 5). Principally, this isotopic variation in the La Pacana rocks could result from wall-rock assimilation and simultaneous crystallization of the andesite–dacite magma (AFC) or it could result from mixing between dacite and an isotopically more primitive mafic magma. For La Pacana, we favor the mixing hypothesis because the chemically most evolved rhyolites (Toconao ignimbrite) are isotopically similar to the associated dacites (Atana ignimbrite) and can be related to them by fractional crystallization (Lindsay et al. 2000). An AFC process would produce more assimilation as fractionation progresses. In a study of the nearby Lascar andesite–dacite stratovolcano, Matthews et al. (1994) suggested that only the relatively hot andesitic magmas (890–970 °C) evolved by an AFC process whereas a flattening of the $^{87}Sr/^{86}Sr$ versus Sr trend was observed for compositions at ~60 wt% SiO_2. A dominance of fractionation over assimilation is expected to be even greater for the cooler La Pacana dacites (~760 °C; Lindsay 1999).

The La Pacana, Purico, and Chascon–Aspero dome magmas clearly have crustal isotopic signatures, but the isotopic variations among them suggest that the crustal contribution decreased with time between 4.1 (La Pacana) and < 0.5 Ma (Chascon–Aspero). Source heterogeneities are unlikely to explain this variation because all centers are in close proximity, and particularly so for the Purico and Chascon-Aspero domes (Fig. 2). Mixing calculations indicate that the Purico compositions could be produced by adding ~30% of basaltic andesite, as represented by the mafic inclusions in Chascon–Aspero lavas, to the most "crustal" high-$^{87}Sr/^{86}Sr$ magma from the La Pacana complex (Cerro Bola dacite dome; Lindsay et al. 2000). Using the same end-members, the proportion of basaltic andesite in the Chascon dacites would be ~60% whereas even the most primitive Sr isotope ratio in the La Pacana dacites requires < 20% basaltic andesite. These values are minimum estimates for the proportion of mafic components in the different magmas because the "crustal" end-member, Cerro Bola dacite, may itself be a hybrid magma and not a pure crustal melt.

A rough upper limit of the depth of crustal melting beneath the APVC region can be derived from the REE characteristics of the Purico and other APVC ignimbrites. These show no evidence for the heavy REE depletion that would result from equilibration of melts with residual garnet (i.e., $La/Yb_n > 20$). Experimental melting studies show that garnet is produced by incongruent melting of biotite in quartzo-feldspathic compositions at pressures >1.25 GPa (Patiño-Douce and Beard 1995), and the lack of a garnet signature in the REE data thus suggests that melting took place at depths of < ~30 km. A further constraint on the upper limit of magma generation comes from considering the

data trend in the Sr isotopic diagram (Fig. 5). The trajectory defined by the Purico and La Pacana data in this diagram is close to a simple mixing trend, although an AFC process would seem far more likely because interaction between mafic magmas and cooler crustal melts must involve simultaneous crystallization of the former. If AFC is envoked, the data trend in Fig. 5 requires that the bulk distribution coefficient for Sr during fractionation of the mafic magma, D_{Sr}, is close to 1. This value varies with the relative proportion of clinopyroxene and plagioclase in the fractionating assemblage, which is pressure sensitive. To demonstrate this, we calculated the proportions of plagioclase and clinopyroxene produced by crystallization of a typical arc basaltic andesite (Leon Muerto in Trumbull et al. 1999) at different pressures, using the MELTS software of Ghiorso and Sack (1995) and assuming 2 wt% H_2O at the Ni–NiO buffer. At pressures <500 MPa ($\sim$15 km) plagioclase fractionation is important (50% of solid phases), Sr behaves as a compatible element ($D_{Sr}=1.35$ using partition coefficients in Tables 8, 9, and 10), and the AFC model predicts a strong depletion in Sr with increasing crustal assimilation. For higher pressures, >700 MPa ($\sim$20 km), clinopyroxene dominates during the first 50% fractionation (forming $\sim$75% of solid phases) and this causes a bulk distribution coefficient near 1 ($D_{Sr}=0.93$), similar to a mixing trend. The latter is consistent with the isotopic trend for the most primitive compositions (lowest 1/Sr in Fig. 5), suggesting that magma interaction took place at depths $>\sim$20 km, but we note that this trend is also affected by secondary fractionation and magma mixing.

Thus the isotopic and trace element characteristics of the ignimbrites suggest that crustal melting and AFC interaction with mafic arc magma occurred in mid-crustal levels between 35 and 15 km. Adopting the model of de Silva (1989a) and Laube and Springer (1998), we envisage a mid-crustal ponding of arc-derived basalt–andesite magmas as the dominant mechanism for generating the ignimbrite magmas. Geophysical observations (low s-wave velocities and high electrical conductivity; Schmitz et al. 1997; Chmielowski et al. 1999) provide good evidence that a partially molten zone exists today beneath the Altiplano-Puna plateau at $\sim$20 km depth. This may be the present manifestation of the mid-crustal source for the APVC ignimbrites. Crustal melting and hybridization with andesites must have been active since at least 10 Ma, the onset of ignimbrite activity in the APVC. The peak activity of large-volume ignimbrite volcanism in the APVC ceased with the $\sim$4 Ma La Pacana and Guacha caldera-forming events, and younger activity is more sporadic and much smaller in volume. As described above, the proportion of mantle-derived magma in the La Pacana, Purico, and Aspero–Chascon systems appears to increase with time, and therefore the Purico system may represent the waning stages of a major crustal melting event and a return to the dominance of more basic magmas from the active arc.

Conclusions

The Pleistocene ignimbrites and post-ignimbrite lava domes of the Purico complex in northern Chile represent one of the few silicic ignimbrite centers in the central Andes where compositional zoning can be linked to mafic recharge. The initial ignimbrite eruption at Purico (LPI I) tapped homogeneous, crystal-rich dacite. During the following LPI II event, a relatively hot crystal-poor rhyolite was deposited first in a highly explosive eruption, followed by dacite, which was tapped along with minor amounts of compositionally distinct andesites. Post-ignimbrite lava domes are dacitic and also contain andesitic clasts. The andesite, dacite, and rhyolite pumices from the zoned LPI II units have indistinguishable Sr and Nd isotopic compositions ($\epsilon Nd=-6.7$ to -7.2 and $^{87}Sr/^{86}Sr=0.7085$–0.7090), but petrological and geochemical evidence indicate that they do not represent a simple fractionation sequence. The dacites seem to have equilibrated at 4–8 km depth and moderate temperatures (780 °C) under water-saturated conditions ($\sim$4 wt% H_2O). The pre-eruptive temperature of the rhyolite is hotter than the dacite and trace element data from melt inclusions and matrix glass indicate that the dacite magma is too evolved to be the source of the rhyolite. Compositional patterns of zoned plagioclase in the rhyolite indicate strong local temperature gradients in the magma.

To explain these features we envisage injection of fresh andesite into the dacitic magma chamber between the LPI I and LPI II eruptions. Thermal and chemical disequilibrium with dacite promoted rapid crystallization and effective fractionation of andesite to rhyolite. The hot, low density and low viscosity rhyolitic melt was able to ascend without significant equilibration with the resident dacite. The ascent and concomitant decompression of this volatile-rich rhyolite is a likely trigger for the plinian eruption, which marks the beginning of the LPI II ignimbrite.

The isotopic composition of Purico units suggest that all magmas are hybrid with varying degrees of crustal and arc-derived mantle components. Mixing calculations based on Sr isotopic ratios indicate a minimum proportion of 30% arc-derived basaltic andesite in the ignimbrites, and a decreasing crustal contribution with time.

Acknowledgements Funding for this study was provided by the Deutsche Forschungsgemeinschaft in the framework of the collaborative research center SFB 267 "Deformation processes in the Central Andes". We thank Moyra Gardeweg, SERNAGEOMIN Chile and colleagues from the Universidad Católica del Norte in Antofagsta for logistical help and advice during field work. For their help with analytical work we are grateful to our colleagues from the GeoForschungsZentrum Potsdam, in particular Rudi Naumann (XRF), Erika Kramer (REE), Wolfgang Siebel (Sr- and Nd-isotopes), Dieter Rhede and Oona Appelt (EPMA), and Peter Dulski (LA-ICP-MS). Renate Karstädt skillfully drafted the geological map of Purico on the basis of field and remote sensing data. Some microprobe analyses were done at the University of Giessen with the help and advice of Rüdiger Borchardt. Rick Hervig, Kurt

Roggensack and other members of the geology department at Arizona State University (ASU) are thanked for their hospitality during a 6-month stay of A.K.S. and invaluable advice in doing SIMS analysis on melt inclusions. The visit to ASU was made possible by a grant to A.K.S. from the Deutscher Akademischer Austauschdienst. Reviews by Charles Bacon and an anonymous journal reviewer helped clarify this presentation.

Analytical procedures

For determining pumice and lava crystallinity, X-ray diffraction (XRD) spectra of the samples and of reference materials of known crystal-content were compared. Reference materials were prepared by mixing powders of natural minerals plagioclase, quartz and hornblende, and natural aphyric rhyolitic glass. Mineral phases were quantitatively determined after Emmermann and Lauterjung (1990). Relative 2σ errors on major mineral phase and glass abundance are generally between 5 and 10%. Densities of selected pumice and lava samples were determined by weighing clasts in air and water following the Houghton and Wilson (1989). Dense rock equivalent density was determined by He-pycnometry on fine-grained rock powders (<63 μm) of compositionally similar samples. The vesicularity of each clast was then calculated from the measured density differences. Phenocryst, microlite, and glass compositions of all pumice and lava types were determined using electron microprobe analysis (EPMA), secondary ionization mass spectrometry (SIMS), laser ablation mass spectrometry with inductively coupled plasma (LA-ICP-MS) and infrared spectroscopy (FTIR). For EPMA of glasses, a 10-nA beam at 15 kV accelerating voltage was rastered over a 20-μm^2 area to minimize Na loss. 1σ errors (%rel) of EPMA analysis based on 32 replicate analyses on natural rhyolitic glass: $SiO_2 = 0.3$, $TiO_2 = 10.0$, $Al_2O_3 = 6.1$, $Fe_2O_3 = 5.6$, $MnO = 21.4$, $MgO = 8.3$, $CaO = 3.3$, $K_2O = 1.1$, $Na_2O = 1.4$, $P_2O_5 = 50.0$. SIMS spot analyses on glasses and step-scans on plagioclase were made on a modified Cameca 3f ion microprobe at Arizona State University and on a Cameca 6f ion microprobe at the GeoForschungsZentrum Potsdam with an instrumental set-up described in Ihinger et al. (1994). Standard materials used were NBS610 and NBS612 glasses for trace elements and experimentally synthesized hydrous rhyolite glasses with water determined by Karl–Fischer titration (Westrich 1987). 1σ errors (% rel) of SIMS analysis based on counting statistics and instrumental background (for H_2O): $H_2O = 0.15$ wt% (abs.), $Rb = 4.7$, $Sr = 6.2$, $Y = 6.0$, $Nb = 11.0$, $Ba = 2.5$, $La = 14.0$, $Ce = 8.7$, $Th = 17.0$, $U = 18.0$. LA-ICP-MS mineral analyses were carried out at the GeoForschungsZentrum Potsdam using an UV-Microprobe attached to a PQS-S ICP-mass-spectrometer by VG-Elemental (see Schmitt 1999 for analytical details). For details of X-ray fluorescence (XRF), ICP-MS, emission spectroscopy (ICP-OES) and conventional mass spectrometry (TIMS) procedures the reader is referred to Trumbull et al. (1999) and Schmitt et al. (2000).

References

Ahrens TA (ed) (1995) A handbook of physical constants: Mineral physics and crystallography, vol 2. American Geophysical Union, Washington, DC, pp 1–354

Anders E, Grevesse N (1989) Abundances of the elements; meteoritic and solar. Geochim Cosmochim Acta 53:197–214

Andersen DJ, Lindsley DH (1988) Internally consistent solution models for Fe–Mg–Mn–Ti oxides; Fe–Ti oxides. Am Mineral 73:714–726

Andersen DJ, Lindsley DH, Davidson PM (1993) QUILF: a Pascal program to assess equilibria among Fe–Mg–Mn–Ti oxides, pyroxenes, olivine, and quartz. Comp Geosci 19:1333–1350

Anderson JL, Smith DR (1995) The effects of temperature and fO_2 on the Al-in-hornblende barometer. Am Mineral 80:549–559

Bacon CR, Druitt TH (1988). Compositional evolution of the zoned calcalkaline magma chamber of Mount Mazama Crater Lake Oregon. Contrib Mineral Petrol 98:224–256

Bacon CR, Hirschmann MM (1988) Mg/Mn partitioning as a test for equilibrium between coexisting Fe–Ti oxides. Am Mineral 73:57–61

Best MG, Christiansen EH, Deino AL, Gromme CS, Tingey DG (1995) Correlation and emplacement of a large, zoned, discontinuously exposed ash flow sheet; the $^{40}Ar/^{39}Ar$ chronology, paleomagnetism, and petrology of the Pahranagat Formation, Nevada. J Geophys Res B 100:24593–24609

Blake S (1990) Viscoplastic models of lava domes. In: Fink JH (ed) Lava flows and domes; emplacement mechanisms and hazard implications. Springer, Berlin Heidelberg New York, pp 88–126

Blake S, Ivey GN (1986a) Magma-mixing and the dynamics of withdrawal from stratified reservoirs. J Volcanol Geotherm Res 27:153–178

Blake S, Ivey GN (1986b) Density and viscosity gradients in zoned magma chambers and their influence on withdrawal dynamics. J Volcanol Geotherm Res 30:201–230

Blundy JD, Wood BJ (1991) Crystal-chemical controls on the partitioning of Sr and Ba between plagioclase feldspar silicate melts and hydrothermal solutions. Geochim Cosmochim Acta 55:193–209

Bottinga Y, Weill D, Richet P (1982) Density calculations for silicate liquids. I Revised method for aluminosilicate compositions. Geochim Cosmochim Acta:46:909–919

Campbell IH, Turner JS (1986) The influence of viscosity in fountains in magma chambers. J Petrol 27:1–30

Carey S, Sigurdsson H (1989) The intensity of plinian eruptions. Bull Volcanol 51:28–40

Carey S, Sparks RSJ (1986) Quantitative models of the fallout and dispersal of tephra from volcanic eruption columns. Bull Volcanol 48:109–125

Chmielowski J, Zandt G, Haberland C (1999) The central Andean Altiplano–Puna magma body. Geophys Res Lett 26:783–786

Davidson JP, de Silva SL, Holden P, Halliday AN (1990) Small-scale disequilibrium in a magmatic inclusion and its more silicic host. J Geophys Res B 95:17661–17675

de Silva SL (1989a) Altiplano–Puna volcanic complex of the central Andes. Geology 17:1102–1106

de Silva SL (1989b) Geochronology and stratigraphy of the ignimbrites from the 21°30′ S to 23°30′ S portion of the central Andes of northern Chile. J Volcanol Geotherm Res 37: 93–131

de Silva SL (1989c) The origin and significance of crystal rich inclusions in pumices from two Chilean ignimbrites. Geol Mag 126:159–175

de Silva SL (1991) Styles of zoning in central Andean ignimbrites; insights into magma chamber processes. In: Harmon RS, Rapela CW (eds) Andean magmatism and its tectonic setting, Geol Soc Am Spec Pap 265:233–243

de Silva SL, Francis PW (1991) Volcanoes of the central Andes. Springer, Berlin Heidelberg New York, 216 pp

de Silva SL, Self S, Francis PW, Drake RE, Ramirez RC (1994) Effusive silicic volcanism in the central Andes; the Chao Dacite and other young lavas of the Altiplano–Puna volcanic complex. J Geophys Res B 99:17805–17825

Droop GTR (1987) A general equation for estimating Fe^{3+} concentrations in ferromagnesian silicates and oxides from microprobe. Mineral Mag 51:431–437

Dunn T, Sen C (1994) Mineral/ matrix partition coefficients for orthopyroxene plagioclase and olivine in basaltic to andesitic systems; a combined analytical and experimental study. Geochim Cosmochim Acta 58:717–733

Eichelberger JC, Izbekov PE (2000) Eruption of andesite triggered by dike injection: contrasting cases at Karymsky Volcano, Kamchatka and Mt Katmai, Alaska. Philos Trans R Soc Lond 358:1465–1485

Eichelberger JC, Chertkoff DG, Dreher ST, Chrisopher JN (2000) Magmas in collision: rethinking chemical zonation in silicic magmas. Geology 28:603–606

Elston WE (1984) Mid-Tertiary ash flow tuff cauldrons, southwestern New Mexico. J Geophys Res B 89:8733–8750

Emmermann R, Lauterjung J (1990) Double X-ray analysis of cuttings and rock flour: a powerful tool of rapid and reliable determination of borehole lithostragraphy. Sci Drill 1:269–282

Ewart A, Griffin WL (1994) Application of proton-microprobe data to trace-element partitioning in volcanic rocks. Chem Geol 117:251–284

Folch A, Marti J (1998) The generation of overpressure in felsic magma chambers by replenishment. Earth Planet Sci Lett 163:301–314

Francis PW, Baker MCW (1978) Sources of two large ignimbrites in the central Andes; some Landsat evidence. J Volcanol Geotherm Res 4:81–87

Francis PW, McDonough WF, Hammill M, O'Callaghan LJ, Thorpe RS (1984) The Cerro Purico shield complex north Chile. In: Harmon RS, Barreiro BA (eds) Andean magmatism; chemical and isotopic constraints. Shiva Publications, Kent, pp 106–123

Francis PW, Sparks RSJ, Hawkesworth CJ, Thorpe RS, Pyle DM, Tait SR, Mantovani MSM, McDermott F (1989) Petrology and geochemistry of volcanic rocks of the Cerro Galan caldera northwest Argentina. Geol Mag 126:515–547

Gans PB, Mahood GA, Schermer ER (1989) Synextensional magmatism in the Basin and Range Province; a case study from the eastern Great Basin. Geol Soc Am Spec Pap 233:1–53

Gardeweg M, Ramirez CF (1987) La Pacana Caldera and the Atana ignimbrite; a major ash-flow and resurgent caldera complex in the Andes of northern Chile. Bull Volcanol 49:547–566

Ghiorso MS, Sack RO (1995) Chemical mass transfer in magmatic processes. IV, A revised and internally consistent thermodynamic model for the interpolation and extrapolation of liquid–solid equilibria in magmatic systems at elevated temperatures and pressures. Contrib Mineral Petrol 119:197–212

Hawkesworth CJ, Hammill M, Gledhill AR, van Calsteren P, Rogers G (1982) Isotope and trace element evidence for late-stage intra-crustal melting in the High Andes. Earth Planet Sci Lett 58:240–254

Hildreth W (1981) Gradients in silicic magma chambers; implications for lithospheric magmatism. J Geophys Res B 86:10153–10192

Holland JD, Blundy TJB (1994) Calcic amphibole equilibria and a new amphibole–plagioclase geothermometer. Contrib Mineral Petrol 104:208–224

Holtz F, Johannes W (1994) Maximum and minimum water contents of granitic melts: implications for chemical and physical properties of ascending magmas. Lithos 32:149–159

Houghton BF, Wilson CJN (1989) A vesicularity index for pyroclastic deposits. Bull Volcanol 51:451–462

Housh TB, Luhr JF (1991) Plagioclase-melt equilibria in hydrous systems. Am Mineral 76:477–492

Huppert HE, Sparks RSJ, Turner JS (1984) Effects of volatiles on mixing in calc-alkaline magma systems. Nature 297:554–557

Huppert HE, Sparks RSJ, Whitehead JA, Hallworth MA (1986) Replenishment of magma chambers by light inputs. J Geophys Res B 91:6113–6122

Ihinger PD, Hervig RL, McMillan PF (1994) Analytical methods for volatiles in glasses. In: Carroll MR, Holloway JR (eds) Volatiles in Magmas Rev Mineral 30:67–121

Johnson MC, Rutherford, MJ (1989) Experimentally determined conditions in the Fish Canyon Tuff, Colorado, magma chamber. J Petrol 30:711–737

Keppler H, Wyllie PJ (1990) Role of fluids in transport and fractionation of uranium and thorium in magmatic processes. Nature 348:531–533

Lange RA (1994) The effect of H_2O, CO_2 and F on the density and viscosity of silicate melts. In: Carroll MR, Holloway JR (eds) Volatiles in magmas. Rev Mineral 30:331–369

Laube N, Springer J (1998) Crustal melting by ponding of mafic magmas; a numerical model. J Volcanol Geotherm Res 81:19–35

Lindsay JM (1999) Geology and magmatic evolution of large volume felsic ignimbrites of the La Pacana caldera central Andes Chile. PhD Thesis, University of Giessen. Sci Tech Rep 99/16, GeoForschungsZentrum Potsdam

Lindsay JM, Schmitt AK, Trumbull RB, de Silva SL, Siebel W, Emmermann R (2000) Magmatic evolution of the La Pacana Caldera system, central Andes, Chile: compositional variation of two cogenetic, large-volume felsic ignimbrites and implications for contrasting eruption mechanisms. J Petrol (in press)

Lindsley DH (1983) Pyroxene thermometry. Am Mineral 68:477–493

Lipman PW (1997) Subsidence of ash-flow calderas: relation to caldera size and magma-chamber geometry. Bull Volcanol 59:198–218

Lipman PW, Doe BR, Hedge CE, Steven TA (1978) Petrologic evolution of the San Juan volcanic field. Southwestern Colorado; Pb and Sr isotope evidence. Geol Soc Am Bull 89:59–82

Lu F, Anderson AT, Davis AM (1995) Diffusional gradients at the crystal/melt interface and their effect on the composition of melt inclusions. J Geol 103:591–597

Lucassen F, Franz G, Thirlwall M, Metzger K (1999) Crustal recycling of metamorphic basement: late Paleozoic granites of northern Chile (~22°S) Implications for the composition of the Andean crust. J Petrol 40:1527–1551

Matthews SJ, Jones AP, Gardeweg MC (1994) Lascar Volcano northern Chile; evidence for steady-state disequilibrium. J Petrol 35:401–432

McDowell FW, Clabaugh SE, Elston WE (1979) Ignimbrites of the Sierra Madre Occidental and their relation to the tectonic history of western Mexico. In: Chapin CE, Elston WE (eds) Ash-flow tuffs. Geol Soc Am Spec Pap 180:113–124

Ort MH, Coira BL, Mazzoni MM (1996) Generation of a crust–mantle magma mixture; magma sources and contamination at Cerro Panizos central Andes. Contrib Mineral Petrol 123:308–322

Patiño-Douce AE, Beard JS (1995) Dehydration-melting of biotite gneiss and quartz amphibolite from 3 to 15 kbar. J Petrol 36:707–738

Pinkerton H, Stevenson RJ (1992) Methods of determining the rheological properties of magmas at sub-liquidus temperatures. J Volcanol Geotherm Res 53:47–66

Roedder E (1984) Fluid inclusions. Rev Mineral 30:646

Scaillet B, Holtz F, Pichavant M (1998) Phase equilibrium constraints on the viscosity of silicic magmas. 1. Volcanic–plutonic comparison. J Geophys Res B 103:27257–27266

Schmitt AK (1999) Melt generation and magma chamber processes in the Purico complex and implications for ignimbrite formation in the Central Andes. PhD Thesis, University of Giessen. Sci Tech Rep 99/18 GeoForschungsZentrum Potsdam

Schmitt AK, de Silva SL (2000) The Merzbacher and Eggler (1984) geohygrometer: a cautionary note on its suitability for high-K suites. J Petrol 41:357–362

Schmitt AK, Emmermann R, Trumbull RB, Bühn B, Henjes-Kunst F (2000) Petrogenesis and $^{40}Ar/^{39}Ar$ geochronology of the

Brandberg complex Namibia: evidence for a major mantle contribution in metaluminous and peralkaline granites. J Petrol 41:1207–1239

Schmitz M, Heinsohn WD, Schilling FR (1997) Seismic, gravity and petrological evidence for partial melt beneath the thickened central Andean crust (21–23°S). Tectonophysics 270:313–326

Schumacher JC (1997) The estimation of ferric iron in electron microprobe analysis of amphiboles. Mineral Mag 61:312–321

Shaw HR (1972) Viscosities of magmatic silicate liquids; an empirical method of prediction. Am J Sci 272:870–893

Singer BS, Dungan MA, Layne GD (1995) Textures and Sr, Ba, Mg, Fe, K and Ti compositional profiles in volcanic plagioclase clues: to the dynamics of calc-alkaline magma chambers. Am Mineral 80:776–798

Sisson TW, Bacon CR (1999) Gas-driven filter pressing in magmas. Geology 27:613–616

Smith RL (1979) Ash-flow magmatism. In: Chapin CE, Elston WE (eds) Ash-flow tuffs. Geol Soc Am Spec Pap 180:5–27

Sparks RSJ, Francis PW, Hamer RD, Pankhurst RJ, O'Callaghan LO, Thorpe RS, Page R (1985) Ignimbrites of the Cerro Galan Caldera, NW Argentina. J Volcanol Geotherm Res 24:205–248

Tepley FJ III, Davidson JP (1997) Recharge in volcanic systems; evidence from isotope profiles of phenocrysts. Science 275:826–829

Trumbull RB, Wittenbrink R, Hahne K, Emmermann R, Büsch. W, Gerstenberger H, Siebel W (1999) Evidence for Late Miocene to Recent contamination of arc andesites by crustal melts in the Chilean Andes 25–26°S and its geodynamic implications. J S Am Earth Sci 12:135–155.

Watts RB, de Silva SL, Jimenez de Rios G, Croudace I (1999) Effusive eruption of viscous silicic magma triggered and driven by recharge: a case study of the Cerro Chascon–Runtu Jarita Dome complex in southwest Bolivia. Bull Volcanol 60:241–264.

Westrich HR (1987) Determination of water in volcanic glasses by Karl–Fischer titration. Chem Geol 63:335–340

Wilson L, Walker GPL (1987) Explosive volcanic eruptions VI. Ejecta dispersal in plinian eruptions: the control of eruption conditions and atmospheric properties. Geophys J Royal Astrom Soc 89:657–679

Wolff JA, Wörner G, Blake S (1990) Gradients in physical parameters in zoned felsic magma bodies; implications for evolution and eruptive withdrawal. J Volcanol Geotherm Res 43:37–55